













## MYC-driven gliosis impairs neuron-glia communication in amyotrophic lateral sclerosis

Paolo V. Fioretti,<sup>1,†</sup> Anna Barbieri,<sup>1,†</sup> Alice Migazzi,<sup>1,†</sup>  Davide Bressan,<sup>1</sup> Maurizio Grassano,<sup>2,3</sup> Luisa Donini,<sup>1</sup> Michela Rocuzzo,<sup>1,4</sup> Maria Claudia Torrieri,<sup>2</sup> Francesca Conci,<sup>1</sup> Elisa Ferracci,<sup>1</sup> Sabrina Invernizzi,<sup>5</sup> Katie M. Bowden,<sup>6</sup> Francesca Bacchetti,<sup>7</sup> Sara Cappelli,<sup>8</sup> Daniele Peroni,<sup>1,9</sup> Romina Belli,<sup>1,9</sup> Michael Pancher,<sup>1,10</sup> Vera Mugoni,<sup>1</sup> Giorgina Scarduelli,<sup>1,4</sup> Matteo Giancesello,<sup>1</sup> Laura Pasetto,<sup>11</sup> Giulia Canarutto,<sup>8,12</sup> Serena Carra,<sup>13</sup> Alessia Soldano,<sup>14</sup> Alessandra Bisio,<sup>1</sup> Sergio Robbiati,<sup>1,15</sup> Chiara Valentini,<sup>1,16</sup> Caterina Nardella,<sup>1</sup> Silvano Piazza,<sup>8,12</sup> Vito G. D'Agostino,<sup>1</sup>  Alessandro Quattrone,<sup>1</sup> Sama Sleiman,<sup>17</sup> Jonathan R. Whitfield,<sup>18</sup> Laura Soucek,<sup>18,19,20,21</sup> Beatrice Vignoli,<sup>1</sup> Gabriella Viero,<sup>22</sup> Luca Tiberi,<sup>1</sup> Alessio Zippo,<sup>1</sup>  Francesca Demichelis,<sup>1</sup>  Valentina Bonetto,<sup>11</sup> Marco Milanese,<sup>7,23</sup> Emanuele Buratti,<sup>8</sup> Federico Verde,<sup>24,25</sup>  Nicola Ticozzi,<sup>24,25</sup>  Andrea Calvo,<sup>2,26</sup>  Antonia Ratti,<sup>5,24</sup>  Pamela J. Shaw,<sup>6,27</sup> Marco Terenzio,<sup>28</sup> Fulvio Chiacchiera,<sup>1</sup>  Maria Pennuto<sup>29,30</sup> and  Manuela Basso<sup>1</sup>

<sup>†</sup>These authors contributed equally to this work.

Chronic activation of glial cells leads to the dysfunction and degeneration of motor and cortical neurons in amyotrophic lateral sclerosis and frontotemporal dementia with an unknown mechanism.

To shed light on the molecular pathogenetic processes underlying the exordium and contribution of gliosis to disease onset and progression, we used cells, mice and patient-derived cells modelling TDP-43, SOD1 and C9ORF72-linked and sporadic ALS.

Our data reveal a sequential disease progression, starting with enhanced glial reactivity and proliferation, and transitioning into inflammation with upregulation of pro-inflammatory genes. Using mouse genetics, we show that expression of mutant TDP-43 in astrocytes is necessary to cause gliosis and behavioural abnormalities. Mechanistically, we show that glial MYC gain-of-function drives neurodegeneration by promoting the release of astrocyte-derived extracellular vesicles that nonetheless fail to provide trophic support to surrounding neurons.

Our research reveals a novel functional role for MYC in glia-to-neuron miscommunication in ALS.

- 1 Department of Cellular, Computational and Integrative Biology (CIBIO), University of Trento, Trento 38123, Italy
- 2 'Rita Levi Montalcini' Department of Neuroscience, ALS Centre, University of Turin, Turin 10126, Italy
- 3 National Institute of Neurological Disorders and Stroke, National Institutes of Health, Bethesda, MD 20892, USA
- 4 Department CIBIO, Advanced Imaging Core Facility (AICF), University of Trento, Trento 38123, Italy
- 5 Department Medical Biotechnology and Translational Medicine, Università degli Studi di Milano, Milan 20122, Italy

Received December 16, 2024. Revised July 28, 2025. Accepted August 30, 2025. Advance access publication September 26, 2025

© The Author(s) 2025. Published by Oxford University Press on behalf of the Guarantors of Brain.

This is an Open Access article distributed under the terms of the Creative Commons Attribution-NonCommercial License (<https://creativecommons.org/licenses/by-nc/4.0/>), which permits non-commercial re-use, distribution, and reproduction in any medium, provided the original work is properly cited. For commercial re-use, please contact [reprints@oup.com](mailto:reprints@oup.com) for reprints and translation rights for reprints. All other permissions can be obtained through our RightsLink service via the Permissions link on the article page on our site—for further information please contact [journals.permissions@oup.com](mailto:journals.permissions@oup.com).

- 6 Sheffield Institute for Translational Neuroscience, School of Medicine and Population Health, University of Sheffield, Sheffield S10 2HQ, UK
- 7 Department of Pharmacy, Pharmacology and Toxicology Unit, University of Genoa, Genoa 16132, Italy
- 8 International Centre for Genetic Engineering and Biotechnology, Trieste 34149, Italy
- 9 Department CIBIO, Proteomics and Mass Spectrometry Core Facility (MS), University of Trento, Trento 38123, Italy
- 10 Department CIBIO, High Throughput Screening and Validation Core Facility (HTS), University of Trento, Trento 38123, Italy
- 11 Research Center for ALS, Istituto di Ricerche Farmacologiche Mario Negri IRCCS, Milan 20156, Italy
- 12 Department of Life Sciences, University of Trieste, Trieste 34127, Italy
- 13 Department of Biomedical, Metabolic and Neural Sciences, University of Modena and Reggio Emilia, Modena 41125, Italy
- 14 Department of Neuroscience, Scuola Internazionale Superiore di Studi Avanzati (SISSA), Trieste 34136, Italy
- 15 Department CIBIO, Model Organism Core Facility (MOF), University of Trento, Trento 38123, Italy
- 16 Department CIBIO, Next Generation Sequencing Core Facility (NGS), University of Trento, Trento 38123, Italy
- 17 Department of Biological Sciences, Lebanese American University, PO Box 36, Byblos, Lebanon
- 18 Vall d'Hebron Institute of Oncology, Cellex Centre, Hospital University Vall d'Hebron Campus, Barcelona 08035, Spain
- 19 Institució Catalana de Recerca i Estudis Avançats, Barcelona 08010, Spain
- 20 Department of Biochemistry and Molecular Biology, Universitat Autònoma de Barcelona, Bellaterra 08193, Spain
- 21 Peptomyc S.L., Barcelona 08035, Spain
- 22 CNR Unit Trento, Institute of Biophysics, Trento 38123, Italy
- 23 IRCCS Ospedale Policlinico San Martino, Genoa 16132, Italy
- 24 Department of Neurology and Laboratory of Neuroscience, IRCCS Istituto Auxologico Italiano, Milan 20145, Italy
- 25 Department of Pathophysiology and Transplantation (DEPT), Dino Ferrari Center, Università degli Studi di Milano, Milan 20122, Italy
- 26 Azienda Ospedaliero-Universitaria Città della Salute e della Scienza di Torino, SC Neurologia 1U, Turin 10126, Italy
- 27 The NIHR Sheffield Biomedical Research Centre, Sheffield Teaching Hospitals NHS Foundation Trust, Sheffield S10 2JF, UK
- 28 Molecular Neuroscience Unit, Okinawa Institute of Science and Technology Graduate University, Okinawa 904-0495, Japan
- 29 Department of Biomedical Sciences (DBS), University of Padova, Padova 35131, Italy
- 30 Veneto Institute of Molecular Medicine (VIMM), Padova 35129, Italy

Correspondence to: Manuela Basso

Department of Cellular, Computational and Integrative Biology-CIBIO

University of Trento, Via Sommarive 9, Trento 38123, Italy

E-mail: manuela.basso@unitn.it

**Keywords:** astrocytes; amyotrophic lateral sclerosis; TDP-43; gliosis; MYC; extracellular vesicles

## Introduction

Neurodegenerative diseases are, in most cases, incurable conditions with common phenotypic and mechanistic features. At the molecular level, mitochondrial dysfunction, excitotoxicity, protein quality control disruption, RNA metabolism alterations and gliosis have been observed in nearly all conditions. However, the causes or consequences of these pathological processes remain unknown. Gliosis manifests as temporal phenotypic and functional changes in astrocytes, oligodendrocytes and microglia cells,<sup>1–4</sup> and it was initially reported by anatomopathological studies of post-mortem brains from individuals with chronic pathologies, such as Alzheimer's disease (AD),<sup>5</sup> Parkinson's disease (PD),<sup>6</sup> frontotemporal dementia (FTD)<sup>7</sup> and amyotrophic lateral sclerosis (ALS),<sup>8</sup> as well as in acute conditions like stroke and traumatic brain injury.<sup>9</sup> These findings were based on the expression of glial acidic fibrillary protein (GFAP), a structural astrocytic protein whose synthesis is increased upon gliosis.<sup>4</sup> Acute neurodegenerative diseases are characterized by a glial proliferative phase followed by inflammation, while chronic neurodegenerative conditions are characterized

by elevated expression and release of pro-inflammatory mediators.<sup>2</sup> Increasing evidence shows that neuroinflammation plays a crucial role in the development and progression of neurodegenerative diseases. However, treatments intended to block inflammatory signalling pathways have not been successful,<sup>10</sup> suggesting that the molecular mechanisms mediating gliosis in chronic neurodegenerative diseases have not been fully uncovered or that the optimal treatment time frame needs to be better defined.

ALS is the most common chronic motor neuron disease that begins in adulthood and gradually affects motor neurons in the motor cortex, brainstem and spinal cord.<sup>11,12</sup> ALS is a highly heterogeneous disease, both clinically and genetically. At early stages, patients show motor impairments in different districts of the body, and the disease may progress in 3–5 years to up to 20 years.<sup>13</sup> ALS can be sporadic or familial, linked most frequently to gene mutations such as *SOD1*, *C9orf72*, *TARDBP* and *FUS*.<sup>12</sup> A hallmark observed in 97% of ALS cases is the presence of intracellular inclusions enriched with TAR DNA-binding protein 43 (TDP-43).<sup>14</sup> This RNA-binding protein also accumulates in 50% of FTD cases<sup>14</sup> and 57% of AD and PD cases.<sup>15,16</sup> A key pathogenic process

underlying ALS is the miscommunication among neighbouring cells.<sup>17</sup> Co-culture experiments with glia and neurons, or assemblages composed of glia, neurons and muscle cells, showed that the expression of mutant superoxide dismutase (SOD1), TDP-43 and C9ORF72 in specific non-neuronal cell types drives neuronal death.<sup>18</sup> Accordingly, the selective removal of mutant SOD1 from astrocytes, oligodendrocytes or microglia of a transgenic ALS mouse model at the embryonic stage significantly slowed disease progression and increased the lifespan of ALS mice.<sup>19–21</sup> Although these observations imply a key role for astrocytes in ALS, how the expression of disease-linked proteins in astrocytes causes motor neuron dysfunction and degeneration is unknown.

Emerging evidence has revealed that glia-neuron communication relies on the release of extracellular vesicles (EVs). When EVs reach the target cell, they first dock to the plasma membrane and afterwards can trigger signalling by activating surface receptors, be internalized by the cell through endocytosis or fuse completely with the target cell.<sup>22,23</sup> *In vitro* research shows that EVs from glial cells expressing ALS-linked mutant SOD1 exacerbate motor neuron degeneration.<sup>24–26</sup> Furthermore, inhibiting overall exocytosis, including EV release, worsened symptoms in an ALS mouse model expressing mutant TDP-43,<sup>27</sup> while blocking non-traditional protein secretion reduced toxicity in C9ORF72, TARDBP, FUS and sporadic ALS models, both *in vitro* and *in vivo*.<sup>28</sup> Furthermore, EVs are considered potential biomarkers because they are consistently released into biofluids and carry proteins and nucleic acids that reflect the pathological state of their originating cells.<sup>29,30</sup> These findings suggest that disruptions in EV-mediated cell-to-cell communication contribute to ALS pathogenesis. However, the link between gliosis, EV function and pathology remains to be clarified.

Here, we show that increased GFAP expression occurs concomitantly with motor neuron degeneration during the early stages of ALS and precedes the onset of glial inflammation. Elevated GFAP levels are associated with enhanced astrocyte proliferation and increased phosphorylated MYC. Dysregulation of MYC activity in ALS triggers the release of altered astrocyte-derived EVs that lose their physiological ability to support neighbouring neurons. Finally, changes in brain-specific EV populations are detected in the CSF of patients with ALS at diagnosis, pointing to potential novel biomarkers for monitoring the different disease stages.

## Materials and methods

A detailed version of the 'Materials and methods' section is provided in the [Supplementary material](#).

## Results

### Transient astrocyte activation at the early symptomatic stage in a TDP-43 mouse model of ALS

We sought to address how gliosis changes as a function of ALS progression. To study the molecular and cellular mechanisms underlying gliosis in ALS, we used transgenic mice expressing human mutant TDP-43<sup>Q331K</sup> flanked by LoxP sites under the control of the prion promoter, leading to TDP-43<sup>Q331K</sup> expression selectively in the CNS and skeletal muscle.<sup>31</sup> These mice exhibit the onset of motor and cognitive dysfunction at 6 months of age, with a progressive increase in severity throughout the lifespan (Fig. 1A).<sup>31,32</sup> Notably, they recapitulate key features of the disease, including gliosis, which is concomitant with the onset of motor symptoms.<sup>31,32</sup> By

immunofluorescence, we detected human TDP-43<sup>Q331K</sup> in neurons, astrocytes and oligodendrocytes, not microglia, as previously reported (Fig. 1B).<sup>32</sup> By analysing the GFAP-positive cells in the spinal cord of TDP-43<sup>Q331K</sup> mice, we confirmed a significant increase of the GFAP signal at 6 months, but surprisingly, not at 10 months (Fig. 1C). To investigate the molecular processes leading to age-dependent gliosis, we immunopurified astrocytes, oligodendrocytes and microglia from the brain of TDP-43<sup>Q331K</sup> mice at the pre-symptomatic stage (3 months), disease onset (6 months) and advanced stage (10 months), and performed RNA sequencing analysis to identify the differentially expressed genes (DEGs) (Fig. 1D–G and [Supplementary Table 1](#)). First, we assessed the purity of each cell population by evaluating the enrichment of specific markers using cytofluorimetry ([Supplementary Fig. 1A](#)) and by comparing the sequencing results with published single-cell analyses<sup>33,34</sup> ([Supplementary Fig. 1B and C](#)). By performing subtractive transcriptome analysis to determine the DEGs at disease onset with respect to the pre-symptomatic stage, we found 113 downregulated and 190 upregulated DEGs in astrocytes (Fig. 1D). We found genes controlling cell proliferation and de-differentiation, including *trans*-acting T-cell-specific transcription factor GATA-3 (*Gata3*),<sup>35</sup> myocyte-specific enhancer factor 2B (*Mef2B*),<sup>36</sup> homeobox protein Hox-C4 (*Hoxc4*),<sup>37</sup> homeobox protein Hox-B3 (*Hoxb3*),<sup>38</sup> serine/threonine-protein kinase PAK 6 (*Pak6*)<sup>39</sup> and paired box protein Pax-1 (*Pax1*)<sup>40</sup> (Fig. 1D). Consistently, among the downregulated DEGs, we found genes that suppress cell proliferation, such as the cyclin-dependent kinase inhibitor 1A (*Cdkn1a*), encoding the CDK inhibitor p21<sup>CIP1</sup>,<sup>41</sup> and RNA-binding motif protein 47 (*Rbm47*), which restrains cell proliferation by inhibiting Wnt/ $\beta$ -catenin signalling.<sup>42,43</sup> Gene ontology (GO) analysis highlighted the deregulation of the transforming growth factor-beta (TGF $\beta$ ) pathway, which is a key regulator of astrogliosis<sup>44,45</sup> and accelerates disease progression in SOD1<sup>G93A</sup> mice, contributing to astrocyte-mediated inflammation<sup>46</sup> (Fig. 1D). In oligodendrocytes at disease onset with respect to the pre-symptomatic stage, we found 282 downregulated and 1443 upregulated DEGs (Fig. 1E and [Supplementary Table 1](#)). Interestingly, the GO analysis of oligodendrocytes highlighted an increase in terms associated with extracellular matrix organization, like yes-associated protein 1 (*Yap1*) and piezo type mechanosensitive ion channel component 1 (*Piezo1*), which mediate cell differentiation and general myelination<sup>47,48</sup> (Fig. 1E).

We then analysed the advanced disease stage to determine whether the cell proliferation and de-differentiation gene signature persists throughout disease progression. At 10 months, we found 296 downregulated and 557 upregulated DEGs in astrocytes. We found a different gene signature at this age, with most of them associated with fibrosis and inflammation (Fig. 1F). The inflammatory state of late-stage astrocytes was further confirmed by the GO analysis, which showed upregulation of terms associated with primary cilium organization and axoneme assembly, typical of C3-positive reactive astrocytes<sup>49</sup> (Fig. 1F). We analysed microglia to determine whether neighbouring cells that do not express the mutant protein also show signs of inflammation. At 10 months, we found 115 downregulated DEGs and 290 upregulated DEGs. CD11b-positive microglia presented a TNF-related inflammatory signature, suggesting that activation of inflammatory pathways is a non-cell-autonomous process (Fig. 1G and [Supplementary Table 1](#)).

Based on these observations, we sought to determine whether active astrocytes show aberrant proliferation *in vivo*. To address this question, we performed an immunohistochemistry assay targeting the proliferation marker Ki-67 in the brain of TDP-43<sup>Q331K</sup> mice (Fig. 2A). We observed comparable levels of Ki-67-positive cells between 3 and 6 months but an overall decrease in cell proliferation

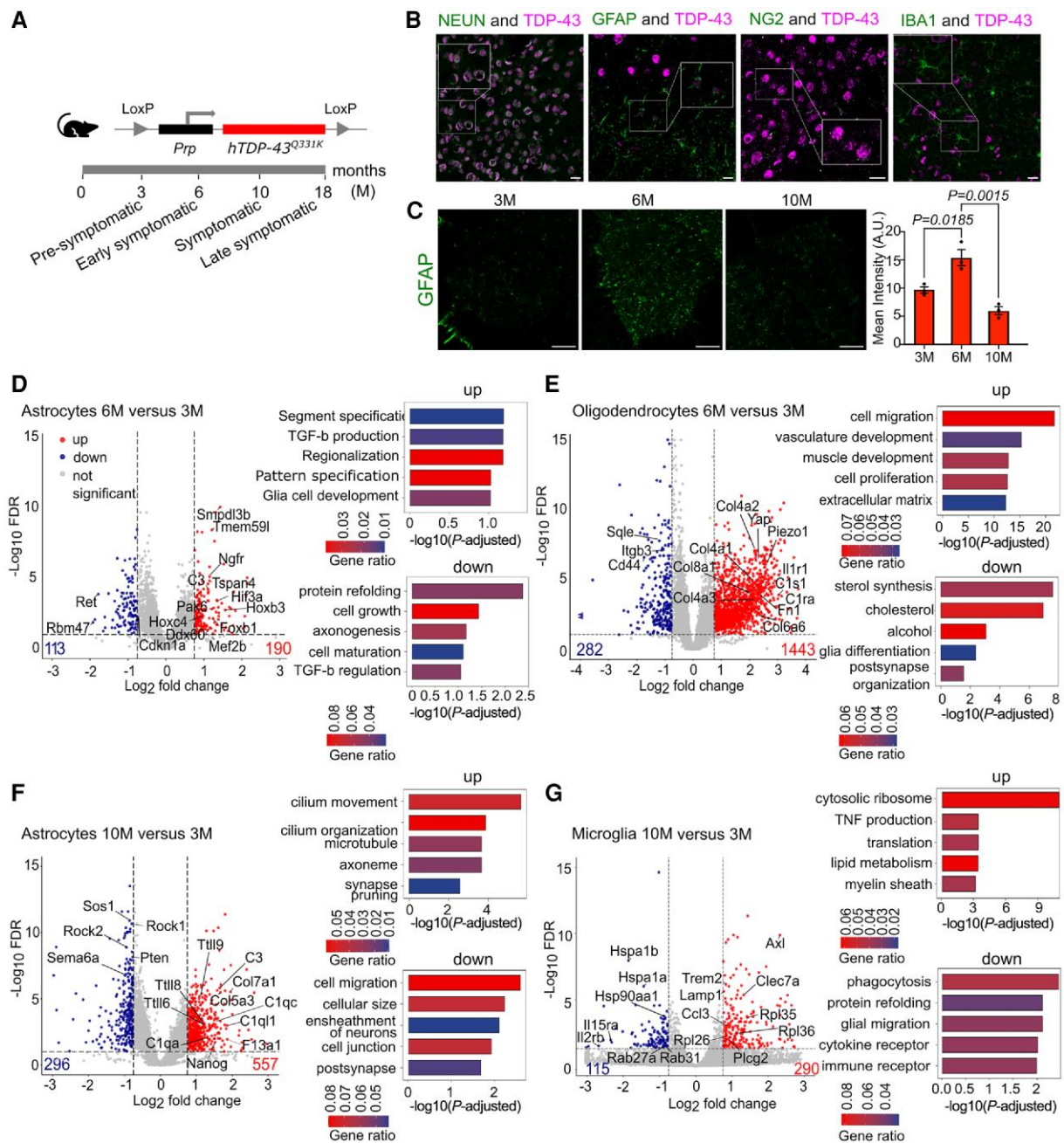


**Figure 1 Proliferative and inflammatory phases of astrocytes in TDP-43<sup>Q331K</sup> mice.** (A) Representative cartoon specifying the time course of the disease in the transgenic TDP-43<sup>Q331K</sup> mouse model. (B) Representative confocal images of 3- to 6-month-old TDP-43<sup>Q331K</sup> mouse brain slices immunostained with antibodies against NEUN (neurons), GFAP (astrocytes), NG2 (oligodendrocytes), IBA1 (microglia) and humanTDP-43<sup>Q331K</sup> (myc-tag). Insets: Magnified (2x) images of selected areas. Scale bars = 20 μm. (C) Representative confocal images (left) and quantification (right) of GFAP expression in the ventral horn of the lumbar spinal cord. Left: Scale bars = 100 μm. Right: Mean ± standard error of the mean; one-way ANOVA analysis followed by Bonferroni's post hoc comparisons (n = 3 mice for each condition). (D) Left: Gene expression volcano plots of astrocytes isolated from the cortices and spinal cord of TDP-43<sup>Q331K</sup> mice at 6 (n = 5 mice) versus 3 (n = 4 mice) months. Up- and downregulated genes were selected with an FDR-corrected P-value threshold of 0.1 and a log<sub>2</sub>FC of 0.75. Right: Gene enrichment analysis from significantly upregulated and downregulated genes in astrocytes isolated from 6- versus 3-month-old TDP-43<sup>Q331K</sup> mice. (E) Left: Gene expression volcano plot of oligodendrocytes isolated from the cortices and spinal cord of TDP-43<sup>Q331K</sup> mice at 6 versus 3 months (n = 4 mice per age). Up- and downregulated genes were selected with an FDR-corrected P-value threshold of 0.1 and a log<sub>2</sub>FC of 0.75. Right: GO term enrichment analysis from significantly upregulated and downregulated genes in oligodendrocytes isolated from 6- versus 3-month-old TDP-43<sup>Q331K</sup> mice. (F) Left: Gene expression volcano plot of astrocytes isolated from the cortices and spinal cord of TDP-43<sup>Q331K</sup> mice at 10 (n = 2 mice) versus 3 (n = 4 mice) months. Up- and downregulated genes were selected with an FDR-corrected P-value threshold of 0.1 and a log<sub>2</sub>FC of 0.75. Right: GO term enrichment analysis from significantly upregulated and downregulated genes in astrocytes isolated from 10- versus 3-month-old TDP-43<sup>Q331K</sup> mice. (G) Left: Gene expression volcano plot of microglia isolated from the brain of TDP-43<sup>Q331K</sup> mice at 10 (n = 4 mice) versus 3 (n = 3 mice) months. Up- and downregulated genes were selected with an FDR-corrected P-value threshold of 0.05 and a log<sub>2</sub>FC of 0.75. Right: GO term enrichment analysis from significantly upregulated and downregulated genes in microglia isolated from 10- versus 3-month-old TDP-43<sup>Q331K</sup> mice. FC = fold-change; FDR = false discovery rate; GO = gene ontology.

at 10 months. To selectively identify proliferating astrocytes, we quantified the number of GFAP<sup>+</sup>/Ki-67<sup>+</sup> cells and found a marked increase in GFAP<sup>+</sup>/Ki-67<sup>+</sup> astrocytes in the brain of 6-month-old TDP-43<sup>Q331K</sup> mice compared to 3-month-old mice, indicating increased proliferation of active astrocytes at disease onset (Fig. 2B).

*In vitro*, cultured astrocytes isolated from post-natal TDP-43<sup>Q331K</sup> mouse brains (Supplementary Fig. 2A and B) exhibited a significant increase in proliferation rate by EdU incorporation (Fig. 2C) compared to wild-type (WT) astrocytes at early passages. Over successive passages, TDP-43<sup>Q331K</sup> primary astrocytes showed a more pronounced decrease in proliferation rate (Fig. 2D) and an upregulation

of the cell cycle inhibitors, *Cdkn1a* and *Cdkn2a*, compared to WT astrocytes (Fig. 2E). These observations indicate that astrocyte activation and proliferation occur concomitantly with the onset of motor dysfunction in a cell-autonomous fashion. Moreover, these pathological processes are transient and followed by inflammation at the fully symptomatic stage.

### TDP-43<sup>Q331K</sup> causes astrogliosis in a cell-autonomous fashion

To assess the relevance of activated astrocytes expressing mutant TDP-43 on the mouse phenotype, we bred the TDP-43<sup>Q331K</sup> mice

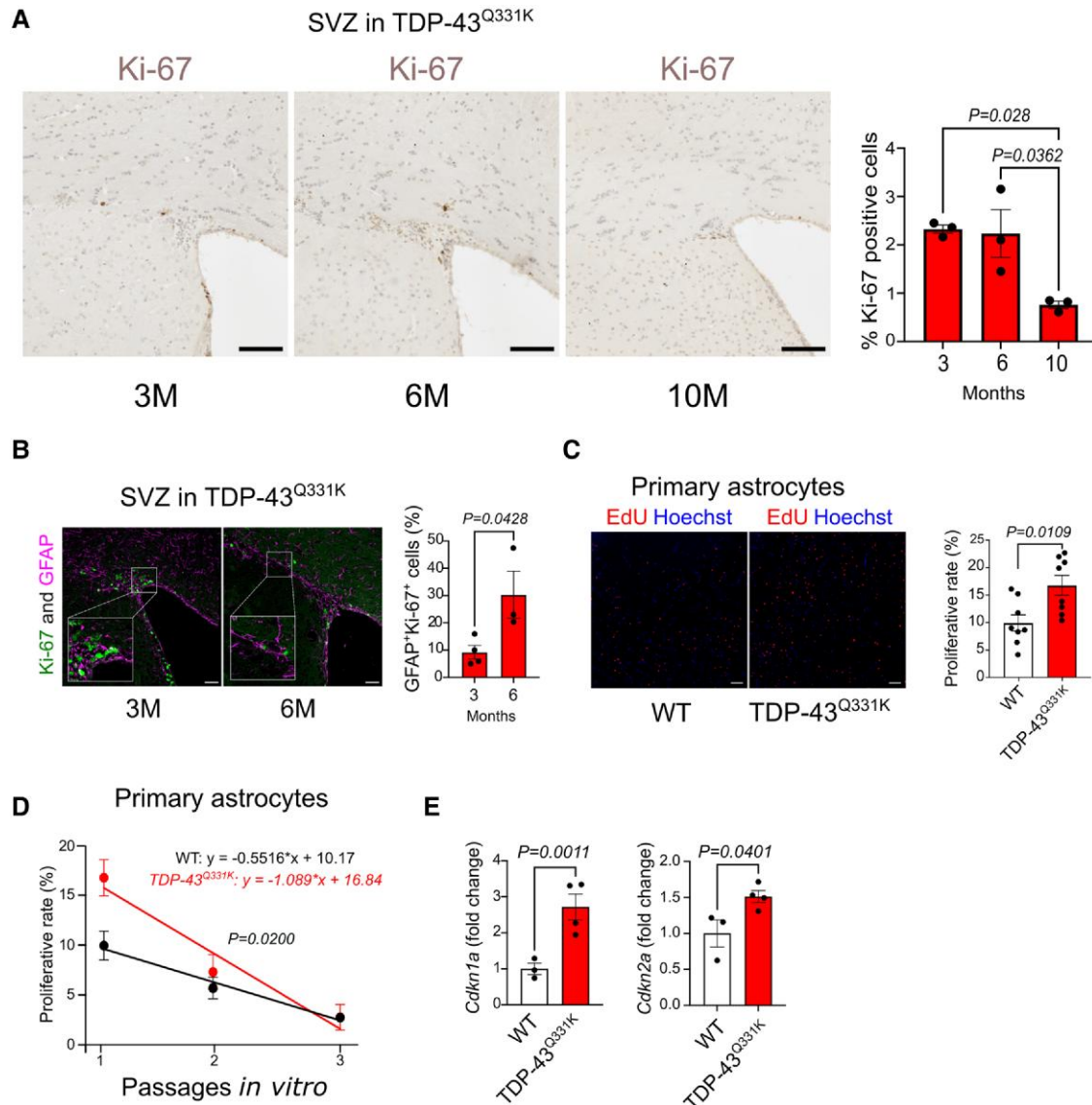


**Figure 2** The proliferative capacity of TDP-43<sup>Q331K</sup> astrocytes is enhanced *in vivo* and *in vitro*. (A) Representative immunohistochemical staining (left) and quantification (right) of Ki-67-positive cells in the brain subventricular zone (SVZ) of TDP-43<sup>Q331K</sup> mice at 3, 6, and 10 months. Normalization was performed on the total number of cells. Mean  $\pm$  SEM; one-way ANOVA analysis followed by Bonferroni's *post hoc* comparisons ( $n=3$  mice). (B) Representative images (left) and quantification (right) of immunofluorescence staining of Ki-67- and GFAP-positive cells in the SVZ of TDP-43<sup>Q331K</sup> mice at 3 ( $n=4$  mice) and 6 ( $n=3$  mice) months. Insets: Magnified (3 $\times$ ) images of selected areas. Left: Scale bars = 50  $\mu$ m. Right: Mean  $\pm$  SEM; unpaired two-sample Student's *t*-test. (C) Representative images (left) and quantification (right) of *in vitro* proliferation assay of wild-type (WT) and TDP-43<sup>Q331K</sup> ( $n=8$  biological replicates) primary astrocytes analysed with EdU staining. Left: Scale bars = 100  $\mu$ m. Right: Mean  $\pm$  SEM; unpaired two-sample Student's *t*-test. (D) Proliferative capacity of WT and TDP-43<sup>Q331K</sup> ( $n=8$  biological replicates) primary astrocytes over three consecutive passages *in vitro*, calculated as the ratio of EdU-positive cells to the total number of cells; simple linear regression analysis. (E) Relative expression of *Cdkn1a* (left) and *Cdkn2a* (right) measured through quantitative real-time PCR in WT ( $n=3$  biological replicates) and TDP-43<sup>Q331K</sup> ( $n=4$  biological replicates) astrocytes after three passages *in vitro*. Mean  $\pm$  SEM; unpaired two-sample Student's *t*-test. SEM = standard error of the mean.

with GLAST-Cre<sup>ERT2</sup> mice for astrocyte-specific expression of tamoxifen-activated Cre recombinase.<sup>50</sup> We then treated the TDP-43<sup>Q331K</sup>xGLAST-Cre<sup>ERT2</sup> mice with tamoxifen at 2 months to allow astrocyte-selective excision of the TDP-43<sup>Q331K</sup> transgene in adult mice (Fig. 3A). In TDP-43<sup>Q331K</sup>xGLAST-Cre<sup>ERT2</sup> mice, transgene excision occurred in astrocytes, not neurons and oligodendrocytes (Fig. 3B and C). Loss of mutant TDP-43 from astrocytes restored the GFAP signal back to normal in the spinal cord of 6-month-old TDP-43<sup>Q331K</sup>xGLAST-Cre<sup>ERT2</sup> mice, indicating that sustained expression of mutant TDP-43 is required for gliosis (Fig. 3D). Next, we evaluated the contribution of astrogliosis to the motor and cognitive phenotypes of this ALS mouse model (Fig. 3A and E–G). We first assessed motor coordination on an accelerated rotarod and muscle strength by the grip strength task in pre-symptomatic mice starting

from 3 months, as previously described.<sup>31</sup> In the rotarod test, both male and female ALS mice showed no overt phenotype in motor dysfunction at 3 months (Supplementary Fig. 3A). In contrast, at 6 months, TDP-43<sup>Q331K</sup> mice developed significant motor deficits that worsened by 10 months (Fig. 3E). Astrocyte-specific ablation of mutant TDP-43 preserved motor coordination up to 6 months, while at 10 months, TDP-43<sup>Q331K</sup>xGLAST-Cre<sup>ERT2</sup> mice performed as TDP-43<sup>Q331K</sup> mice (Fig. 3E). This result was also confirmed by the RNA levels of the nerve growth factor receptor (*Ngfr*) in the gastrocnemius muscle. *Ngfr* is a marker of denervation, specifically expressed by glial cells upon nerve damage at the neuromuscular junctions<sup>51,52</sup> (Supplementary Fig. 3B). *Ngfr* expression significantly increased at 6 months, then decreased at 10 months in TDP-43<sup>Q331K</sup> mice. Accordingly, *Ngfr* levels were significantly upregulated in TDP-43<sup>Q331K</sup>

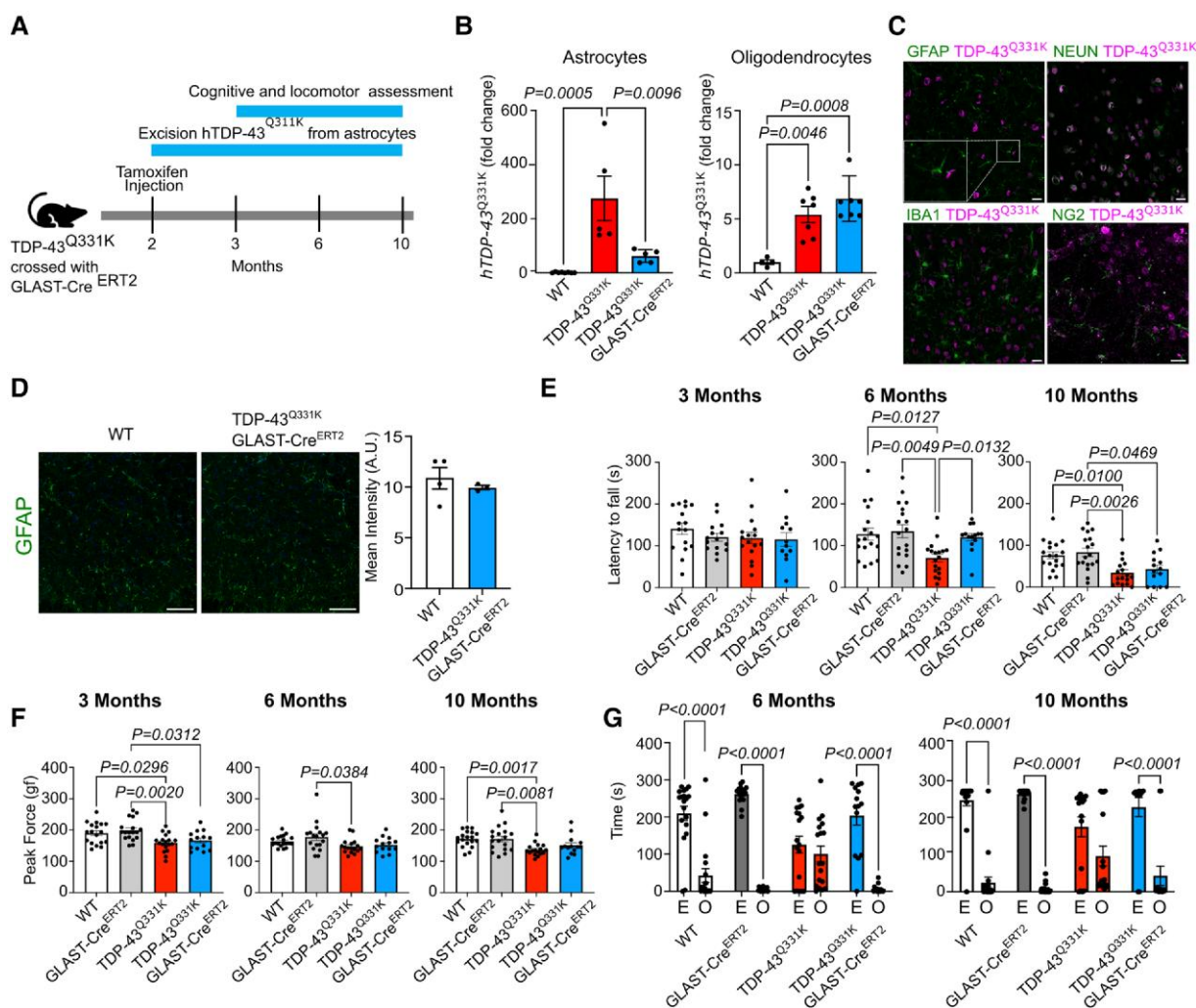


**Figure 3** Reduced astrogliosis correlates with phenotype amelioration in TDP-43<sup>Q331K</sup> mice. (A) Timeline for the behavioural assessments. (B) Relative expression of human TDP-43<sup>Q331K</sup> was measured through quantitative real-time PCR in astrocytes (left) and oligodendrocytes (right) purified from the mouse brain and spinal cord. Astrocytes: WT *n* = 8, TDP-43<sup>Q331K</sup> *n* = 5, TDP-43<sup>Q331K</sup>xGLAST-Cre<sup>ERT2</sup> *n* = 5 biological replicates; oligodendrocytes: WT *n* = 4, TDP-43<sup>Q331K</sup> *n* = 7, TDP-43<sup>Q331K</sup>xGLAST-Cre<sup>ERT2</sup> *n* = 7 biological replicates. Mean ± SEM; one-way ANOVA analysis followed by Bonferroni's post hoc comparisons. (C) Representative confocal images of 3- to 6-month-old TDP-43<sup>Q331K</sup>xGLAST-Cre<sup>ERT2</sup> mouse brain immunostained with antibodies against GFAP (astrocytes), NEUN (neurons), IBA1 (microglia), NG2 (oligodendrocytes) and human TDP-43<sup>Q331K</sup> (myc-tag). Inset: Magnified (2×) image of selected area. Scale bars = 20 μm. (D) Representative confocal images (left) and quantification (right) of GFAP expression in the spinal cord of 6-month-old WT (*n* = 4) and TDP-43<sup>Q331K</sup>xGLAST-Cre<sup>ERT2</sup> (*n* = 3) mice. Left: Scale bars = 100 μm. Right: Mean ± SEM, unpaired two-sample Student's *t*-test. (E–G) Longitudinal study of behaviour: accelerated rotarod, grip strength and elevated plus maze at 3, 6 and 10 months (*n* ≥ 16 WT, *n* ≥ 15 GLAST-Cre<sup>ERT2</sup>, *n* ≥ 16 TDP-43<sup>Q331K</sup>, *n* ≥ 12 TDP-43<sup>Q331K</sup>GLAST-Cre<sup>ERT2</sup> mice). Mean ± SEM, Kruskal–Wallis test followed by Dunn's post hoc comparisons for rotarod and grip strength; mixed-effect analysis followed by Bonferroni's post hoc comparisons for elevated plus maze. SEM = standard error of the mean; WT = wild-type.

xGLAST-Cre<sup>ERT2</sup> mice at 10 months, showing additional evidence of postponed onset of the pathology in mice with astrocyte-specific removal of mutant TDP-43 (Supplementary Fig. 3B).

Muscle strength was slightly but significantly decreased in TDP-43<sup>Q331K</sup> and TDP-43<sup>Q331K</sup>-xGLAST-Cre<sup>ERT2</sup> mice at 3 months, and ablation of TDP-43<sup>Q331K</sup> did not significantly ameliorate this disease feature at 6 and 10 months (Fig. 3F and Supplementary Fig. 3C), suggesting that astrocyte-specific removal of mutant TDP-43 is not sufficient to rescue muscle pathology *in vivo*. Next, we analysed the effect of astrocyte-specific expression of TDP-43<sup>Q331K</sup> on cognitive functions. We analysed disinhibition by exploiting the Elevated Plus Maze test, which quantifies the propensity to spend time in open (O) versus enclosed (E) arms. Mice displaying disinhibition tend to spend more time in the open arms of the maze.<sup>53,54</sup> As previously observed in TDP-43 mice, we detected a significant cognitive decline in TDP-43<sup>Q331K</sup> mice at 6 months compared to age- and sex-matched WT and GLAST-Cre<sup>ERT2</sup> mice (Fig. 3G and Supplementary Fig. 3D). This phenotype was rescued by ablation of TDP-43<sup>Q331K</sup> expression in astrocytes (Fig. 3G). Our results indicate that GFAP increase correlates with symptom onset and progression in TDP-43<sup>Q331K</sup> mice, and that selective removal of TDP-43 from astrocytes delays the onset and slows the progression of the disease.

### Analysis of ALS GWAS reveals transcription factor activity dysregulation centred on MYC

To identify potential factors predisposing glial cells to transient activation and proliferation in patients with ALS, we analysed genome-wide association studies (GWAS) to identify single-nucleotide polymorphisms (SNPs) within transcription factor (TF) binding sites. We used signed linkage disequilibrium profile (SLDP) regression, which focuses on the responsive elements bound by TFs and assesses whether introducing SNP alleles in the DNA sequence increases or decreases TF binding.<sup>55</sup> We ran SLDP regression using 382 available TF annotations<sup>55</sup> on GWAS summary statistics from 29 612 patients with ALS versus 122 656 healthy controls.<sup>56</sup> We detected 40 significant associations at a per-trait false discovery rate (FDR) of <5%. All these associations were positive, suggesting enhanced binding of several TFs, including RE1-silencing transcription factor (REST), rest corepressor 1 (coREST), chromodomain-helicase-DNA-binding protein 2 (CHD2) and specific protein 1 (SP1) (Fig. 4A and Supplementary Table 2), whose increased activity has been previously associated with AD,<sup>57</sup> Huntington's disease<sup>58</sup> and TDP-43 pathology in flies.<sup>59</sup> Among the positive hints, we noticed representative members of the basic helix-loop-helix TF family, namely MYC, a well-known master regulator of cell proliferation, protein translation and cell metabolism, Myc-associated factor X (MAX), which is the c-Myc binding partner, and Max-interacting protein 1 (MXI1), which competes with MYC for binding with MAX.<sup>60</sup> Using STRING to assess predicted protein-protein interactions (<https://string-db.org>), we observed a hub around MYC (Fig. 4B).<sup>60</sup> These results suggested that the activity of MYC is dysregulated in ALS.

To correlate the results of the SLDP regression based on GWAS in patients with ALS to the RNA sequencing analysis performed in TDP-43<sup>Q331K</sup> mice at 3, 6 and 10 months, we took advantage of a computational analysis designed to assess whether alterations in MYC activity influence gene expression. TF activity can be inferred robustly from transcriptomic data.<sup>61</sup> By comparing MYC target genes with the DEGs observed in astrocytes and oligodendrocytes at 6 months versus 3 months, we found a statistically significant impact of MYC activity on gene expression changes (Fig. 4C and D). No

significant correlation was retrieved from DEGs observed in astrocytes and microglia at 10 months versus 3 months in TDP-43<sup>Q331K</sup> mice (Fig. 4E and F). These observations indicated that dysregulation of MYC activity might be responsible for the transitory proliferation of astrocytes at disease onset in TDP-43<sup>Q331K</sup> mice.

### MYC is overactivated in ALS astrocytes and neurons *in vitro*

We next sought to shed light on the role of MYC in ALS. By analysing the levels of c-Myc mRNA by quantitative RT-PCR and RNAscope<sup>®</sup> assay, we found no difference in the mRNA transcript levels in WT and TDP-43<sup>Q331K</sup> astrocytes (Fig. 5A and Supplementary Fig. 4A). Considering the pivotal role of TDP-43 in post-transcriptional regulation of RNA homeostasis,<sup>62</sup> we asked whether c-Myc mRNA stability is affected in TDP-43<sup>Q331K</sup> astrocytes. By RNA immunoprecipitation (RIP) assay in astrocytes expressing either normal or mutant HA-tagged TDP-43, we found that TDP-43<sup>WT</sup> and TDP-43<sup>Q331K</sup> equally bind the c-Myc transcript (Supplementary Fig. 4B). To evaluate the decay rate of c-Myc mRNA in normal and mutant astrocytes, we inhibited transcription by actinomycin D treatment for different time points and measured c-Myc mRNA abundance by quantitative RT-PCR. We detected no significant difference in c-Myc mRNA half-life upon TDP-43<sup>Q331K</sup> expression (Supplementary Fig. 4C). Total MYC protein content was unaffected by mutant TDP-43 expression in primary astrocytes (Fig. 5B). By cycloheximide chase assay, we found no significant change in MYC protein stability in TDP-43<sup>Q331K</sup> astrocytes compared to control astrocytes (Supplementary Fig. 4D). These results indicate that expression of TDP-43<sup>Q331K</sup> does not affect c-Myc transcript and protein levels and stability in astrocytes. We thus asked whether TDP-43<sup>Q331K</sup> modifies MYC activity. Phosphorylation at serine 62 (S62) and threonine 58 (T58) controls both MYC degradation and its binding to chromatin, thereby regulating MYC transcriptional activity.<sup>63–66</sup> To test the correlation between MYC phosphorylation and MYC activity *in vitro*, we expressed phospho-defective (MYC<sup>T58A,S62A</sup>) or phosphomimetic (MYC<sup>T58D,S62D</sup>) mutant MYC in HEK293 cells and in primary astrocytes and performed a transcriptional assay using a reporter vector bearing the firefly luciferase gene under the control of MYC-responsive elements. We observed increased MYC transcriptional activity upon expression of MYC<sup>T58D,S62D</sup> indicating that phosphorylation at S62 and T58 correlates with enhanced MYC transcriptional activity (Fig. 5C and D and Supplementary Fig. 4E). Accordingly, we found significantly increased MYC activity in TDP-43<sup>Q331K</sup> astrocytes and in HEK293 overexpressing TDP-43<sup>WT</sup> compared to control conditions (Fig. 5E and Supplementary Fig. 4F). Using a specific antibody that recognizes MYC when phosphorylated at S62 and T58, we revealed a significant increase of phosphorylated MYC in ALS astrocytes and in HEK cells overexpressing TDP-43<sup>WT</sup> (Fig. 5F and G and Supplementary Fig. 4G). Importantly, phosphorylated MYC was also increased in human-induced neural progenitor cell (NPC)-derived astrocytes directly reprogrammed from fibroblasts donated by two C9ORF72 patients and two patients with sporadic ALS (Fig. 5H).<sup>67</sup>

Finally, we observed a correlation between MYC phosphorylation and the proliferative status of astrocytes *in vitro*. In passage 1 astrocytes, which exhibit higher proliferative capacity (Fig. 2C), phosphorylated MYC is increased (Supplementary Fig. 4H). Conversely, in low proliferative senescent astrocytes at passage three (Fig. 2D and E), phosphorylated MYC is turned off (Supplementary Fig. 4I). Taken together, these results indicate that MYC activity is aberrantly activated in ALS astrocytes.

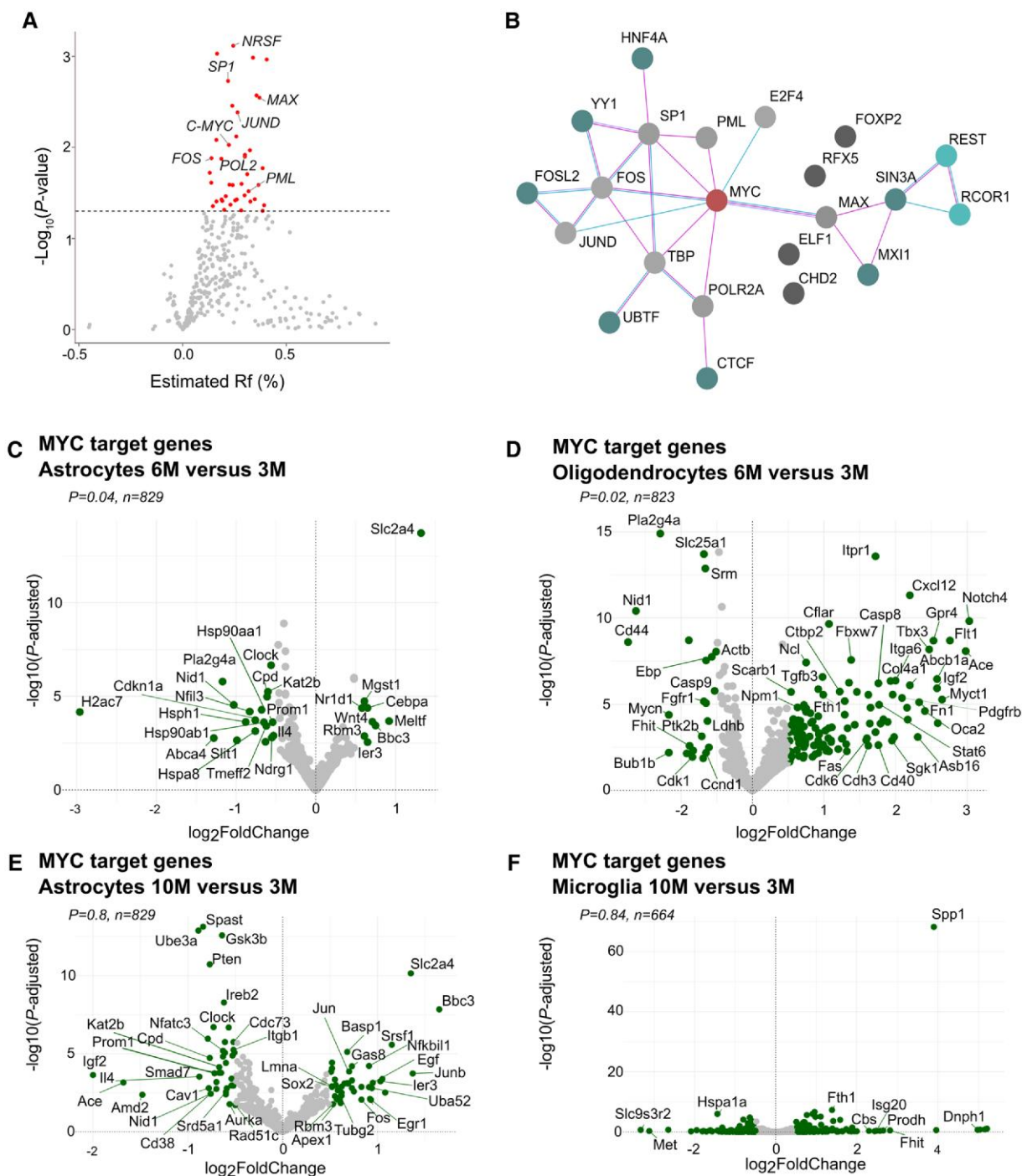


**Figure 4** Transcriptional dysregulation in amyotrophic lateral sclerosis is associated with a MYC-centred hub. (A)  $-\text{Log}_{10}(P)$  against the estimated effect size for the SLDP regression. Red points represent transcription factors with significant associations; non-significant associations are coloured in grey. (B) STRING-generated interaction network among selected enriched KEGG pathways. The network image shows a hub around MYC. (C–F) Green dots represent differentially expressed MYC-target genes in the comparison indicated in the plot’s title ( $\log_2\text{FC} \geq 0.5$  or  $\log_2\text{FC} \leq -0.5$ ,  $P_{\text{adj}} < 0.05$ ). The P-value indicates the significance of MYC inferred activity relative to a random background model (from decoupleR). The MYC targets are the ones defined in the CollecTRI regulons database (see the ‘Materials and methods’ section in the [Supplementary material](#)). FC = fold-change; SLDP = signed linkage disequilibrium profile.

To test whether MYC is also phosphorylated in neurons, as previously reported,<sup>68</sup> we analysed total MYC and activated MYC levels in induced pluripotent stem cell (iPSC)-derived motor neurons from C9ORF72, mutant TDP-43 (TDP-43<sup>M337V</sup>), mutant SOD1 (SOD1<sup>I114T</sup>) or patients with sporadic ALS. The levels of total MYC were

generally unaffected by ALS mutations but increased in the sporadic line ([Supplementary Fig. 5A and B](#)), whereas phosphorylated MYC levels were consistently increased across all ALS conditions ([Supplementary Fig. 5C and D](#)). These results suggest that MYC is usually hyperactivated across different cell types in vivo and

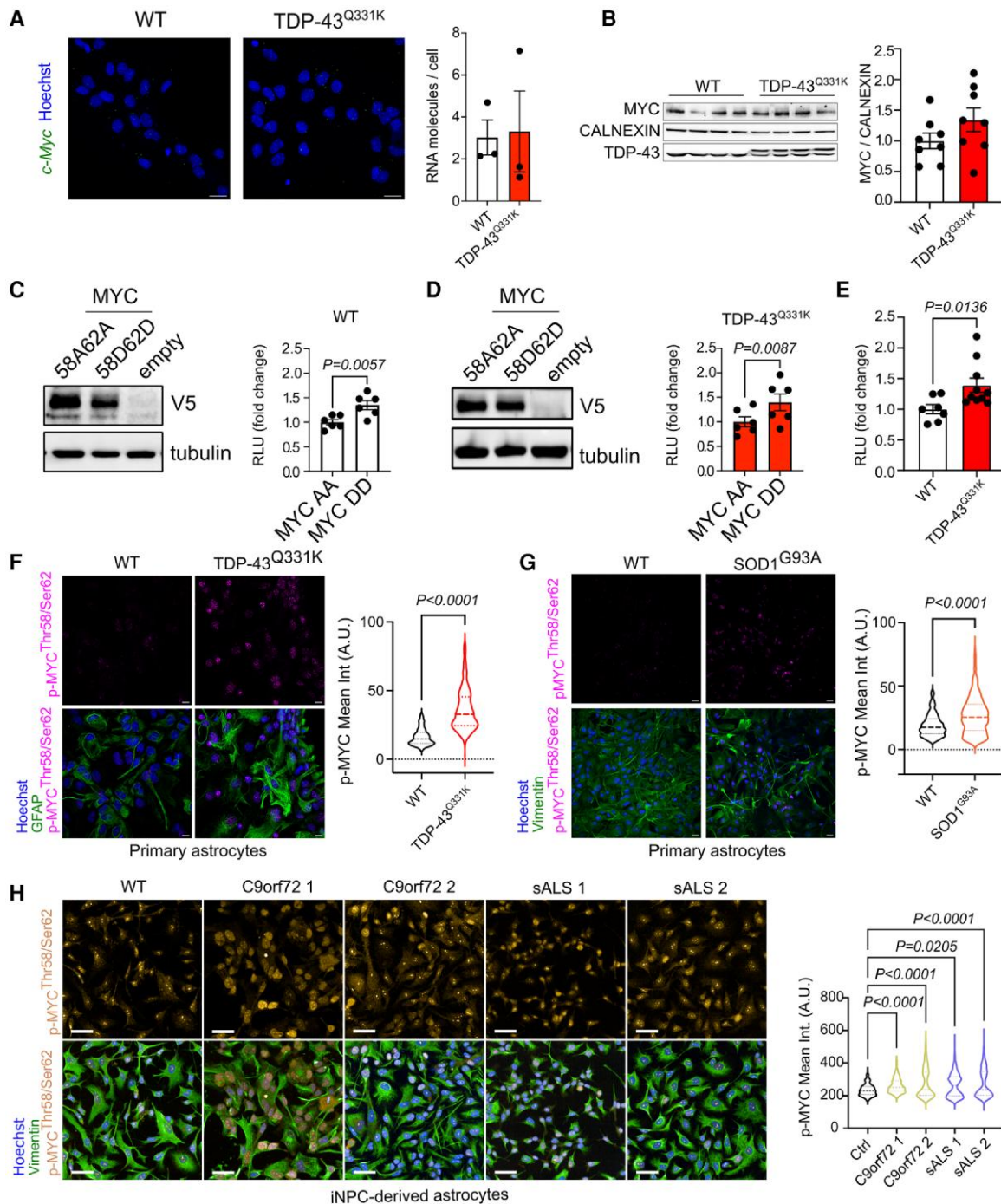


**Figure 5** Phosphorylated MYC is aberrantly increased in astrocytes in several *in vitro* models of amyotrophic lateral sclerosis. (A) Representative confocal images (left) and quantification (right) of *c-Myc* RNA expression in primary astrocytes through RNAscope staining. Left: Scale bar = 20  $\mu$ m. Right: Mean  $\pm$  SEM, unpaired two-sample Student's *t*-test. Data are reported as RNA molecules/cell. ( $n = 3$  biological replicates, with over 400 cells observed per condition). (B) Immunoblotting analysis (left) and quantification (right) of MYC expression in WT and TDP-43<sup>Q331K</sup> primary astrocytes. Right: Mean  $\pm$  SEM, unpaired two-tailed Student's *t*-test ( $n = 8$  biological replicates per genotype). (C and D) Left: Immunoblotting analysis of V5-tagged phospho-defective (58A62A) and phosphomimetic (58D62D) MYC expression in WT (C) and TDP-43<sup>Q331K</sup> (D) primary astrocytes. Right: Luciferase reporter assay showing MYC transcriptional activity in WT (C) and TDP-43<sup>Q331K</sup> (D) primary astrocytes expressing phospho-defective (AA) and phosphomimetic (DD) MYC. Mean  $\pm$  SEM, paired two-tailed Student's *t*-test ( $n = 6$  biological replicates per genotype). (E) Luciferase reporter assay showing MYC transcriptional activity in WT and TDP-43<sup>Q331K</sup> primary astrocytes. Mean  $\pm$  SEM, one-way ANOVA analysis followed by Bonferroni's *post hoc* comparisons ( $n = 7$  biological replicates for WT,  $n = 10$  for TDP-43<sup>Q331K</sup>). (F and G) Representative confocal images (left) and quantification (right) of nuclear signal of primary TDP-43<sup>Q331K</sup> (F) or SOD1<sup>G93A</sup> (G) murine astrocytes immunostained with antibodies against p-MYC<sup>Thr58/Ser62</sup>, GFAP or Vimentin. Scale bars = 10 and 20  $\mu$ m, in F and G, respectively. Mann-Whitney test ( $n = 3$  biological replicates for TDP-43<sup>Q331K</sup> and  $n \geq 4$  for SOD1<sup>G93A</sup>, with over 500 and 1000 nuclei observed per condition, respectively). (H) Representative images (left) and quantification (right) of iNPC-derived astrocytes derived from C9ORF72 or sporadic ALS patients immunostained with antibodies against p-MYC<sup>Thr58/Ser62</sup> and Vimentin. Scale bars = 50  $\mu$ m. Kruskal-Wallis test followed by Dunn's *post hoc* comparisons ( $n = 2$  differentiation replicates for CTRL,  $n = 1$  for C9orf72 1,  $n = 3$  for C9orf72 2,  $n = 3$  for sALS 1,  $n = 3$  for sALS 2, with over 240 nuclei observed per condition). iNPC = induced pluripotent stem cell-derived neural progenitor cell; sALS = sporadic amyotrophic lateral sclerosis; SEM = standard error of the mean; WT = wild-type.

in vitro models of ALS, validating the prediction of the SLDP regression performed on GWAS data.

### Overactivated MYC in astrocytes mimics TDP-43<sup>Q331K</sup>-induced neurodegeneration

To assess the impact of overactivated MYC in ALS, we crossed the TDP-43<sup>Q331K</sup> × GLAST-Cre<sup>ERT2</sup> mice with R26StopFLMYC mice carrying a floxed STOP cassette that prevents the expression of c-MYC (Fig. 6A). Upon tamoxifen injection, we generated mice with astrocyte-specific overexpression of MYC in the absence of TDP-43<sup>Q331K</sup> (Supplementary Fig. 6A). If MYC activation is a downstream effect of TDP-43 gain of function in ALS, we would expect to observe motor neuron damage in the triple transgenic mice (MYC-Stop<sup>fl</sup> × TDP-43<sup>Q331K</sup> × GLAST-Cre<sup>ERT2</sup>). First, we investigated neuronal degeneration by performing Nissl staining in the spinal cord to assess motor neuron loss. As expected, starting at symptom onset around 6 months, TDP-43<sup>Q331K</sup> mice showed a reduction in healthy motor neurons along with an increase in enlarged motor neurons with cytoplasmic vacuolization<sup>69</sup> (Fig. 6B and C and Supplementary Fig. 6B). On the contrary, TDP-43<sup>Q331K</sup> × GLAST-Cre<sup>ERT2</sup> mice maintained a high number of healthy neurons at 6 months (Fig. 6B and C), consistent with improved motor performance in the rotarod test upon mutant TDP-43 removal from astrocytes, as shown in Fig. 3E. In MYC-Stop<sup>fl</sup> × TDP-43<sup>Q331K</sup> × GLAST-Cre<sup>ERT2</sup> mice, which exhibit astrocyte-specific TDP-43<sup>Q331K</sup> depletion and concurrent c-MYC overexpression, motor neurons show an enlarged morphology and signs of induced neurotoxicity, mimicking the phenotype observed in TDP-43<sup>Q331K</sup> mice. Secondly, we measured neurofilament light chain (NFL), a well-established biomarker of motor neuron degeneration.<sup>70</sup> NFL is increased in TDP-43<sup>Q331K</sup> mice at 6 months (Fig. 6D). Astrocyte-specific ablation of TDP-43<sup>Q331K</sup> reduced plasma NFL levels, whereas c-MYC overexpression increased NFL levels and dramatically reduced lifespan (Fig. 6D and E).

To exclude the fact that these mice died earlier because of glioblastoma, we analysed the expression of Ki-67 in the brain as a tumour marker. We included a validated model of medulloblastoma with combined OTX2 and c-MYC overexpression as a positive control,<sup>71</sup> where we found an evident Ki-67 staining at the level of the tumour. However, we did not detect any signal in mice with astrocyte-specific overexpression of c-MYC alone or c-MYC/TDP-43<sup>Q331K</sup> together (Supplementary Fig. 6C).<sup>72</sup>

Taken together, these results indicate that MYC overexpression in astrocytes is sufficient to cause motor neuron toxicity *in vivo* and suggest that MYC acts downstream of TDP-43<sup>Q331K</sup> in astrocytes to cause motor neuron dysfunction and premature death.

### MYC inhibition in TDP-43<sup>Q331K</sup> astrocytes reveals MYC-dependent transcription driving gliosis

To map the downstream pathways affected by MYC hyperactivation in ALS astrocytes, we cultured primary astrocytes from TDP-43<sup>Q331K</sup> mice and treated them with Omomyc, a dominant-negative mini-protein that halts MYC binding to chromatin.<sup>73–75</sup> To minimize off-target effects, we titrated Omomyc to determine the minimal effective dose and shortest exposure time required to obtain a significant reduction of MYC transcriptional activity. We treated astrocytes with 20, 40 and 60 μM Omomyc and detected the luciferase signal after 48 and 72 h. As shown in Fig. 6F, treatment with 40 μM Omomyc for 48 h is sufficient to significantly reduce MYC transcriptional activity in TDP-43<sup>Q331K</sup> astrocytes. By bulk RNA sequencing analysis, we observed a significant

modulation of genes involved in lipid transport, such as *Abcg1*, cell chemotaxis, such as *Mmp9*, and several chemokines, namely, *Cxcl2*, *Ccl2* and the small heat shock protein *Hspb1*, all previously investigated in ALS.<sup>76–78</sup> Of relevance, we also report Omomyc-dependent inhibition of *Socs3*, which is directly involved in the activation of the JAK-STAT3 pathway, implicated in astrocyte reactivity and gliosis (Fig. 6G and H and Supplementary Table 3).

These findings support a key role for hyperactivated astrocytic MYC in triggering early astrogliosis as a precursor to inflammation in the TDP-43<sup>Q331K</sup> model.

### Expressing TDP-43<sup>Q331K</sup> or MYC in astrocytes alters common cell communication pathways

To define the specific contribution of increased MYC phosphorylation on the proteome of TDP-43<sup>Q331K</sup> astrocytes, we performed a label-free proteomic analysis on control astrocytes compared to astrocytes expressing TDP-43<sup>Q331K</sup> or MYC. The comparison between WT and TDP-43<sup>Q331K</sup> astrocytes revealed 57 differentially upregulated proteins (Fig. 7A). Remarkably, 54% of the upregulated targets overlapped with the differentially upregulated proteins in WT astrocytes overexpressing MYC (Fig. 7A and Supplementary Table 4). Conversely, a minimal overlap was observed in downregulated proteins, confirming that MYC is a positive regulator of gene transcription that primarily promotes expression of its targets.<sup>60</sup>

The GO analysis of upregulated proteins highlighted an enrichment of biological pathways involved in cell-to-cell interaction and signal transmission (Fig. 7B). The heat map in Fig. 7C (left) shows that several upregulated proteins in TDP-43<sup>Q331K</sup> or MYC-overexpressing astrocytes, such as SIGLEC1, IFITM3 and PAWR, participate in neuroinflammatory events, confirming the results obtained from the transcriptomic analysis on ALS astrocytes treated with Omomyc (Figs 6G and 7C). Other upregulated proteins act as splicing factors (SRSF3, HMG5) or are involved in RNA metabolism and RNA modification (MFAP1a, RBM27), further confirming TDP-43 gain-of-function in this specific ALS/FTD model.<sup>31</sup> The proteomic analysis also revealed an increase in proteins involved in translation (EIF4b, MRPS30) (Fig. 7C). Accordingly, by measuring the total protein amount per cell, we found a higher protein-to-cell ratio in TDP-43<sup>Q331K</sup> astrocytes, indicating increased cell biomass compared to controls (Supplementary Fig. 7A). Finally, among proteins related to intercellular communication, charged multivesicular body protein 2b (CHMP2b), charged multivesicular body protein 4b (CHMP4b), synergin-gamma (SYNRG) and angiomin-like protein 1 (AMOTL1) participate in endosomal formation, multivesicular body (MVB) maturation and vesicular trafficking (Fig. 7C).

MYC has previously been shown to exert a repressive function on lysosome biogenesis,<sup>79</sup> a process that is defective in ALS.<sup>80,81</sup> Consistently, we detected decreased levels of the lysosomal protein LAMP-1 in TDP-43<sup>Q331K</sup> astrocytes by immunoblotting (Supplementary Fig. 7B). When lysosome function is inhibited, cells favour the maturation of MVBs into EVs, resulting in increased EV release as an alternative strategy to remove damaged proteins.<sup>82–85</sup> Changes in EV production or cargo may contribute to the intercellular miscommunication previously described in ALS.<sup>30,86–88</sup> Thus, we tested whether TDP-43<sup>Q331K</sup> astrocytes exhibited altered EV production. We isolated the EVs derived from astrocytes (Supplementary Fig. 7C) and confirmed EV purity by immunoblotting that revealed expression of specific EV markers, but not intracellular markers (Supplementary Fig. 7D).<sup>89</sup> Using cryo-electron microscopy, we detected EVs from both WT and TDP-43<sup>Q331K</sup> astrocytes (Supplementary Fig. 7E). By nanoparticle tracking analysis, we

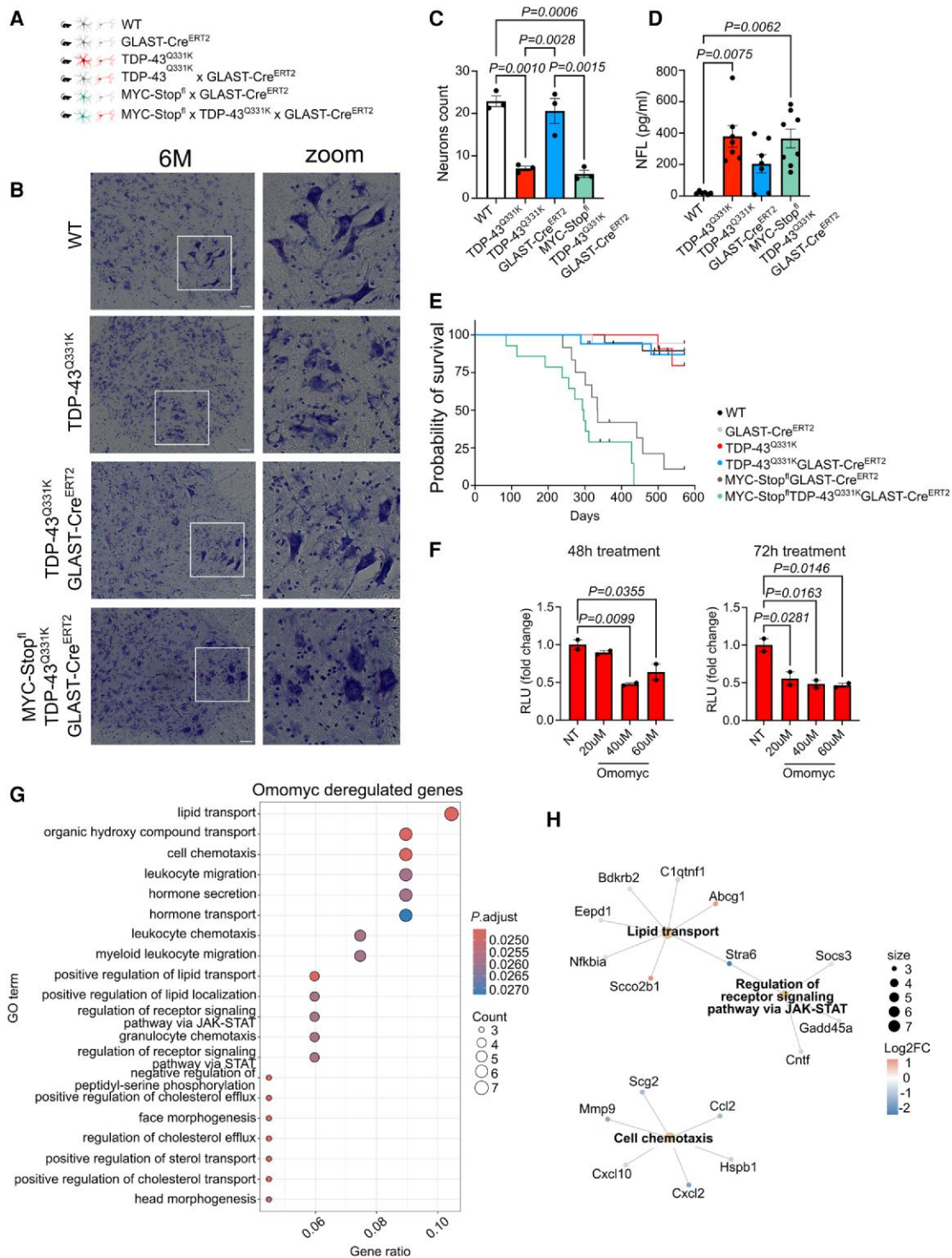


**Figure 6** MYC overactivation mimics TDP-43-induced neurodegeneration, and its inhibition prevents the activation of neuroinflammatory signalling pathways. (A) Representative cartoon specifying mouse lines used in B–E. (B) Representative images (left) showing Nissl staining of motor neurons in the spinal cord of 6-month-old mice. Scale bar = 50  $\mu$ m. Inset: Magnified (3x) image of selected areas. (C) Quantification of the number of neurons with healthy morphology from B. Mean  $\pm$  SEM, one-way ANOVA analysis followed by Bonferroni's *post hoc* comparisons ( $n = 3$  mice per genotype). (D) Plasma NFL levels in 6-month-old mice. Mean  $\pm$  SEM, one-way ANOVA analysis followed by Bonferroni's *post hoc* comparisons ( $n = 6$  WT,  $n = 7$  TDP-43<sup>Q331K</sup>,  $n = 7$  TDP-43<sup>Q331K</sup>GLAST-Cre<sup>ERT2</sup>,  $n = 8$  MYC-Stop<sup>fl</sup>xTDP-43<sup>Q331K</sup>xGLAST-Cre<sup>ERT2</sup> mice). (E) Survival curve of behaviourally tested mice. Kaplan–Meier simple survival analysis. ( $n = 19$  WT,  $n = 18$  GLAST-Cre<sup>ERT2</sup>,  $n = 17$  TDP-43<sup>Q331K</sup>,  $n = 17$  TDP-43<sup>Q331K</sup>GLAST-Cre<sup>ERT2</sup>,  $n = 12$  MYC-Stop<sup>fl</sup>xGLAST-Cre<sup>ERT2</sup>,  $n = 14$  MYC-Stop<sup>fl</sup>xTDP-43<sup>Q331K</sup>xGLAST-Cre<sup>ERT2</sup> mice). (F) Luciferase reporter assay showing MYC transcriptional activity in TDP-43<sup>Q331K</sup> primary astrocytes treated with Omomyc for 48 h (top) and 72 h (bottom). Mean  $\pm$  SEM, one-way ANOVA analysis followed by Bonferroni's *post hoc* comparisons ( $n = 2$  biological replicates). (G) GO term enrichment analysis from significantly deregulated genes ( $\log_2FC \geq 0.5$  and  $\log_2FC \leq -0.5$ ,  $P_{adj} \leq 0.05$ ) in primary astrocytes (TDP-43<sup>Q331K</sup> mice) treated with Omomyc versus vehicle ( $n = 3$  biological replicates per condition). (H) Enrichment by pathway terms visualized using the Gene concept network (cnet plot) function for protein interactions regarding the GOs 'lipid transport', 'regulation of receptor signaling pathway via JAK-STAT' and 'cell chemotaxis' presented in G. FC = fold-change; GO = gene ontology; SEM = standard error of the mean; WT = wild-type.

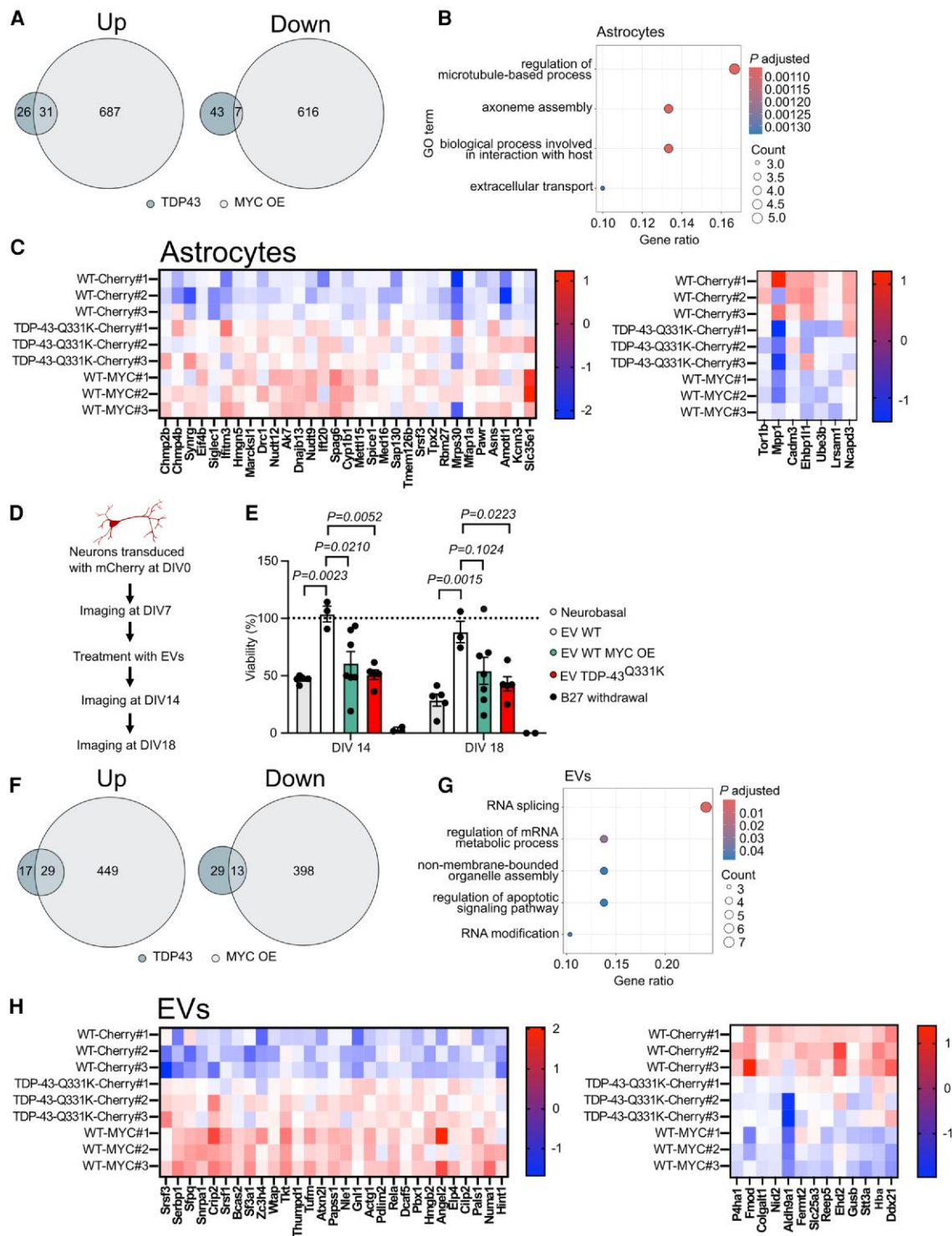


**Figure 7** Increased MYC in TDP-43<sup>Q331K</sup> astrocytes drives the release of altered extracellular vesicles that do not support receiving neurons. (A) Venn diagram depicting common up- and downregulated proteins between TDP-43<sup>Q331K</sup> astrocytes and wild-type (WT) astrocytes overexpressing MYC (WT MYC OE). (B) GO term enrichment analysis from the shared upregulated proteins between the TDP-43<sup>Q331K</sup> astrocyte and the WT astrocyte overexpressing MYC. (C) Heat map representation, based on log<sub>2</sub>-normalized protein abundance, showing the relative abundance of common up- and down regulated proteins (left and right, respectively) between TDP-43<sup>Q331K</sup> and WT astrocytes overexpressing MYC, as measured by quantitative LC-MS/MS-based proteomic analysis. (D) Schematic representation of the neuronal viability experiment. (E) Neuronal survival assay of WT cortical neurons after 7 (DIV14) and 11 (DIV18) days of treatment with extracellular vesicles (EVs) derived from WT, WT MYC OE, and TDP-43<sup>Q331K</sup> astrocytes. Mean ± SEM, two-way ANOVA analysis followed by Tukey's *post hoc* comparisons (n = 2 biological replicates, data are represented as viability percentage in a single field of view). (F) Venn chart representing common up- and downregulated proteins between EVs derived from TDP-43<sup>Q331K</sup> astrocyte or WT astrocyte overexpressing MYC. (G) GO term enrichment analysis from the shared upregulated proteins between EVs from TDP-43<sup>Q331K</sup> astrocytes or WT astrocytes overexpressing MYC. (H) Heat maps showing the relative abundance of common up- and downregulated proteins (left and right, respectively) between EVs derived from TDP-43<sup>Q331K</sup> astrocyte or WT astrocyte overexpressing MYC, as quantified by proteomic analysis. DIV = days *in vitro*; GO = gene ontology; LC-MS/MS = liquid chromatography-tandem mass spectrometry; SEM = standard error of the mean.

quantified the number of EVs produced by WT and TDP-43<sup>Q331K</sup> astrocytes in large EVs and small EVs. We observed a significant increase in small EVs, which mostly derive from MVBs (Supplementary Fig. 7F).<sup>82</sup>

Altogether, these results indicate that the endosomal and lysosomal pathways, along with EV secretion, are altered in TDP-43<sup>Q331K</sup> astrocytes, suggesting that functional communication between astrocytes and nearby neurons might be compromised. Moreover, our proteomic analysis in MYC-overexpressing astrocytes hints towards a role for overactivated MYC in astrocyte-to-neuron miscommunication in the TDP-43<sup>Q331K</sup> ALS model.

### Astrocyte-derived extracellular vesicles fail to support neurons in ALS

To determine the functional consequences of altered EV release, we investigated whether TDP-43<sup>Q331K</sup> astrocyte-derived EVs influence the physiology of receiving neurons. First, we tested if glia EVs could enter primary neurons. After transducing primary astrocytes with CD63-eGFP (Supplementary Fig. 7G) and purifying EVs, we incubated WT neurons with fluorescent-tagged EVs and quantified the signal of internalized EVs (Supplementary Fig. 7H and I). TDP-43<sup>Q331K</sup> and WT astrocyte-derived EVs had a similar propensity to be taken up by receiving cells and enter WT neurons (Supplementary Fig. 7J). To develop reproducible *in vitro* models for neuronal toxicity, we set up an *in vitro* assay to follow neuronal viability over time upon EV treatment (Fig. 7D and Supplementary Fig. 7J). We transduced WT and TDP-43<sup>Q331K</sup> cortical neurons with a lentivirus expressing the fluorescent protein mCherry to image them over time. We performed a first live acquisition at Day *in vitro* (DIV) 7, followed by EV treatment. Live imaging acquisitions were performed at DIV 14 and 18 to verify how the treatment affected neuronal viability. The neuronal count was performed by applying a specific threshold on the mCherry fluorescent signal, using the addition of complete media and B27 removal as control and death conditions, respectively (Supplementary Fig. 7J).

Interestingly, EVs from WT astrocytes exerted a significant pro-survival effect on WT neurons compared to untreated controls at DIV 14 and 18 (Fig. 7E). Conversely, both EVs produced by WT astrocytes overexpressing MYC and EVs derived from TDP-43<sup>Q331K</sup> astrocytes lost this protective effect on WT neurons, indicating that astrocyte-derived EVs have an altered biological effect on nearby neurons (Fig. 7E). Altogether, these results show that alterations in EV release trigger astrocyte-to-neuron miscommunication, resulting in astrocyte loss-of-function and reduced support to neighbouring neurons in the TDP-43<sup>Q331K</sup> ALS model.

To characterize the differential cargo composition of astrocyte-derived EVs, we performed a label-free proteomic analysis in EVs released by control astrocytes, astrocytes expressing TDP-43<sup>Q331K</sup> or MYC. The comparison between WT and TDP-43<sup>Q331K</sup> EVs resulted in 46 differentially upregulated proteins, 63% of which overlapped with the upregulated proteins in EVs secreted by WT astrocytes expressing MYC (Fig. 7F). The GO analysis clearly shows that most of the upregulated targets in EVs released by TDP-43<sup>Q331K</sup>- or MYC-overexpressing astrocytes are linked to RNA processing and RNA modification (Fig. 7G), such as serine/arginine-rich splicing factor 1 (SRSF1) and 3 (SRSF3) (Fig. 7H, left). Interestingly, we also observed a significant increase in factors regulating the apoptotic signalling pathway (e.g. TKT, TUFM, ATXN2L, THUMPD1) (Fig. 7H, left), while among the downregulated cargos (Fig. 7H, right), most of the proteins are constituents of the extracellular matrix,

suggesting possible alterations in the physical interaction between EVs and receiving neurons.

### Extracellular vesicle alterations in the CSF of patients with ALS

We wondered if any of the EV alterations observed in TDP-43<sup>Q331K</sup> primary astrocytes could be retrieved in patients with ALS at the time of diagnosis. We analysed the EVs in the CSF of 19 patients with ALS and 10 patients with hydrocephalus as controls (Supplementary Table 5). We used a multiplex bead-based cytofluorometric assay to provide simultaneous semiquantitative measures of 37 transmembrane proteins commonly expressed in brain-derived EVs<sup>90</sup> (Supplementary Fig. 8A).

First, we examined whether we could detect any differences in established markers specific for EVs released by different cell populations of the nervous system, namely NCAM and PSA-NCAM for neurons, O4 for oligodendrocytes, CD140a for oligodendrocyte precursor cells (OPCs), GLAST for astrocytes and CD11b for microglia (Fig. 8A). The relative levels of NCAM and its post-translationally modified isoform PSA-NCAM were significantly reduced in ALS CSF, along with O4, a marker of mature oligodendrocyte-derived EVs (Fig. 8A). CD140a, also known as platelet-derived growth factor receptor- $\alpha$  (PDGFR $\alpha$ ), is specifically expressed by immature OPCs and was increased in ALS CSF, suggesting an imbalance between mature and immature oligodendrocytes at diagnosis in patients with ALS (Fig. 8A). No significant changes were observed for astrocyte and microglia EVs (Fig. 8A). We then observed that specific EV markers, namely CD9 and CD63, were reduced in the CSF of patients with ALS, supporting the hypothesis that altered MYC activity leads to alterations in EV subpopulations (Fig. 8B). CD47-positive EVs, instead, were significantly enriched in ALS CSF (Fig. 8C). Conversely, we noticed that proteins involved in cell adhesion and signalling to the immune system, such as CD36, CD38, CD44 and CX3CR1, were all decreased in ALS EVs compared to controls, as observed in EVs derived from TDP-43<sup>Q331K</sup> astrocytes (Fig. 8C and D). Integrins or their classical interaction partners showed a similar relative amount in ALS and control CSF (Supplementary Fig. 8B).

Although CSF EVs comprise EVs derived from different neuronal and glial cells, these results confirm a global alteration of EV subpopulations in ALS. The decrease in neuronal and mature oligodendrocyte EVs clearly reflects the pathological situation, while the increase in EVs derived from oligodendrocyte precursors is consistent with our observation of an initial disease phase characterized by glia de-differentiation.

## Discussion

We identified two phases of astrocyte activation in a slowly progressive *in vivo* model of ALS, consistent with previous reports in brain injury models.<sup>91</sup> Astrocytes respond to various pathological insults affecting the CNS, including acute injuries, such as ischaemia, traumatic brain injury, spinal cord injury and infections, as well as progressive disorders, such as neurodegenerative diseases and multiple sclerosis. These responses typically involve changes in cellular morphology and increased expression of intermediate filament proteins, including GFAP and vimentin.<sup>92</sup> In our model, we observed a peak in GFAP expression during the early symptomatic stages, characterized by astrocyte proliferation. Subsequently, GFAP levels decline as the neuroinflammatory response is activated. Accordingly, GFAP immunoreactivity in postmortem ALS

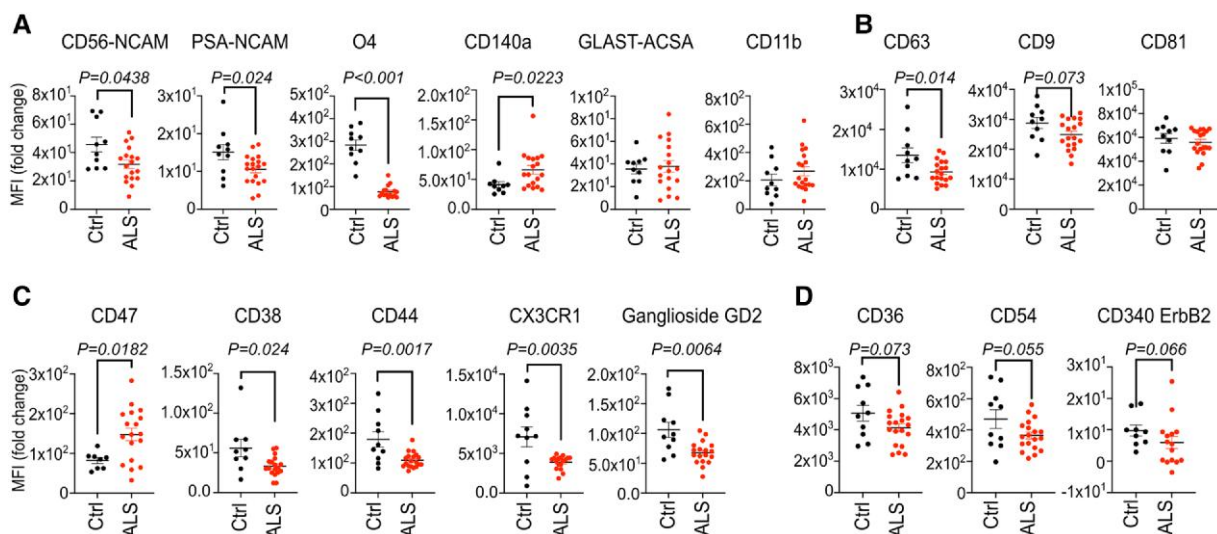


**Figure 8** Altered CSF-derived extracellular vesicle populations in patients with amyotrophic lateral sclerosis. (A–D) Brain-specific extracellular vesicle (EV) markers were measured with the MACSplex EV Kit Neuro in CSF from patients with amyotrophic lateral sclerosis (ALS) and controls (Ctrl). Data are presented in subgroups highlighting: (A) markers of distinct cell populations of the nervous system, (B) EV-specific markers, and (C and D) markers involved in cell adhesion and signalling to the immune system with either a significant difference (C) or a trend (D). The y-axis shows the median fluorescence intensity (MFI, expressed as arbitrary units A.U.) of APC post background correction. Mean  $\pm$  standard error of the mean, unpaired two-tailed Student’s t-test or Mann–Whitney test, depending on normality (n = 10 controls, n = 19 ALS patients).

tissue is comparable to that in healthy controls.<sup>93</sup> Nevertheless, extensive evidence derived from post-mortem studies reports widespread reactive neuroinflammation in ALS.<sup>8,94–96</sup> Astrocyte reactivity upon expression of mutant TARDBP, VCP, SOD1 and C9orf72 has also been confirmed *in vitro* under cell-autonomous conditions.<sup>97</sup> However, the precise timeline of astrocyte phenotypic changes remains poorly understood.

The GWAS analysis we performed on TF binding sites revealed that a network of TFs linked to MYC is predicted to have a deregulated function in ALS, and we further validated MYC as a critical player in astrocyte activation in ALS. Astrocyte reactivity involves a range of transcriptional and functional alterations that are still being explored. The most prominent evidence is that phosphorylated signal transducer and activator of transcription 3 (STAT3) is the master regulator of several reactive astrocyte phenotypes.<sup>98</sup> Increased phosphorylated STAT3 or the upregulation of its downstream targets has been reported in acute and chronic conditions, including ALS.<sup>99</sup> Treatments such as Janus kinase (JAK) inhibitors<sup>100</sup> or niclosamide have been shown to inhibit the STAT3 pathway, reduce gliosis, and exert neuroprotective effects in ALS.<sup>101</sup> Accordingly, the RNA sequencing of Omomyc-treated primary astrocytes showed a direct regulation of Socs3, a well-known inhibitor of the STAT3 pathway.<sup>102</sup> This finding hints at MYC’s role in shaping astroglial as an inflammatory precursor, thereby supporting the concept that astrocyte activation and inflammation represent downstream pathological events in the TDP-43<sup>Q331K</sup> mouse model.

We observed a significant increment of phosphorylated MYC in primary astrocytes derived from transgenic mouse models expressing either human TDP-43<sup>Q331K</sup> or SOD1<sup>G93A</sup> and in induced pluripotent stem cell-derived neural progenitor cell (iNPC)-derived human astrocytes from sporadic ALS cases or presenting a pathological expansion in the C9orf72 gene. c-MYC is one of the most common dysregulated oncogenes in cancer expressing either human TDP-43<sup>Q331K</sup> or SOD1<sup>G93A</sup> and in iNPC-derived human astrocytes from sporadic ALS cases or presenting a pathological expansion in the C9orf72 gene. c-MYC is one of the most common dysregulated

oncogenes in cancer,<sup>60</sup> and its expression is tightly regulated by continuous phosphorylation, ubiquitination and degradation.<sup>103</sup> MYC is phosphorylated by mitogen-activated protein kinases (MAPKs)<sup>104</sup> and dephosphorylated by protein phosphatase 2A (PP2A).<sup>65</sup> Hyperactivation of MAPKs, such as ERK1/2 and p38, has been reported in ALS<sup>105–107</sup> and may contribute to MYC phosphorylation in gliosis. In contrast, PP2A has been reported as inhibited in a transgenic model of AD, showing gliosis.<sup>108</sup> Based on this evidence, we propose that dysregulation of the MAPK pathway or PP2A activity may contribute to the enhanced MYC phosphorylation observed in ALS astrocytes.

Here, we report that phosphorylated MYC is also augmented in ALS motor neurons. We analysed human motor neurons derived from iPSCs carrying mutations in TDP-43, SOD1 and C9ORF72, and those of sporadic patients. We recognize that we used a small number of iPSC lines per condition, with lines derived from control individuals and no isogenic controls, and this represents a limitation in our analyses. Consequently, the increase in phosphorylated MYC observed should be considered as a preliminary indication of MYC alterations in ALS motor neurons, which needs further investigation. However, the results were consistent in all the motor neuronal lines analysed. We speculate that MYC alterations observed in neuronal cells may predispose them to aberrant cell cycle re-entry. Cell cycle re-entry and neuronal de-differentiation have been reported in AD iPSC neurons,<sup>109</sup> and cell-cycle re-entry-induced neuronal death has been associated with DNA damage response in post-mitotic neurons in ageing and AD,<sup>110</sup> traumatic brain injury,<sup>111</sup> ALS and FTD.<sup>112,113</sup> DNA damage response is a common phenomenon observed in ALS, occurring in models carrying mutations in SOD1,<sup>114</sup> C9ORF72,<sup>115,116</sup> FUS<sup>117</sup> and TDP-43.<sup>118</sup> Of interest, DNA damage can activate the transcription factor p53, whose knockout or silencing proved beneficial effects in rescuing C9ORF72 disease models.<sup>119</sup> The involvement of p53, the genome’s guardian, and MYC, the super manager of gene transcription, highlights the relevance of chromatin regulation, TF binding and epigenetic alterations in neurodegenerative diseases like ALS.

We showed that astrocytes expressing mutant TDP-43 fail to support neurons. Contrasting results were reported regarding the impact of mutant TDP-43-expressing astrocytes on neuronal survival.<sup>120–123</sup> In our TDP-43<sup>Q331K</sup> model, we report the inability of astrocyte-derived EVs to support neurons due to a variation in their composition. The loss of pro-survival signals observed in EVs released by transgenic astrocytes correlated with reduced expression of CD44 on the surface of CSF EVs isolated from patients with ALS. CD44 is a membrane glycoprotein involved in several cellular processes, including growth, survival, differentiation and motility.<sup>124</sup> Decreased CD44 levels in CSF-derived EVs from patients with ALS suggest a loss of pro-survival signalling during early phases of the disease. Moreover, CD44 interacts with CD47, CD38, ICAM-1, CD36 and CX3CR1, all of which are associated with regulatory T cells, which are deregulated in ALS.<sup>125</sup>

Alterations in glial-derived EVs in the CSF have been previously reported in a swine model of ALS carrying a mutation in SOD1.<sup>126</sup> Similar to our findings, EVs originating from OPCs were increased at early symptomatic stages and matched with previous reports showing enhanced proliferation of NG2-positive OPCs prior to motor neuron degeneration in SOD1<sup>G93A</sup> mice.<sup>127,128</sup> In contrast, TMEM119, a microglia-specific marker, was augmented only at later phases of the disease,<sup>126</sup> suggesting that monitoring brain-derived EVs in ALS CSF could be helpful in following disease progression. Furthermore, we also reported a decrease in neuron-specific EVs and mature oligo-specific EVs at the time of disease diagnosis. NCAM- and O4-positive EVs, along with CD140a-positive EVs, should be considered for disease progression tracking, paired with the measurement of plasma NFL levels.

In conclusion, our results suggest that astrocyte de-differentiation and proliferation occur before the onset of neuroinflammation in ALS, disrupting the astrocyte-mediated supporting function. Specific biomarkers reflecting these different phases of the disease should be further investigated in patients.

## Data availability

The RNA-seq data discussed in this publication have been deposited in NCBI's Gene Expression Omnibus<sup>129</sup> and are accessible through GEO Series accession number GSE275841 (<https://www.ncbi.nlm.nih.gov/geo/query/acc.cgi?acc=GSE275841>). The mass spectrometry proteomics data have been deposited in the ProteomeXchange Consortium via the PRIDE<sup>130</sup> partner repository with the dataset identifier PXD064120 and 10.6019/PXD064120. Raw data have been uploaded at [https://zenodo.org/records/16320635?token=eyJhbGciOiJIUzUxMiJ9.eyJpZCI6ImI0OTAzMmM1LTBlZWUtNDU5Mi1hODFiLTc4ZGNmNWJlYmRhNSIsImRhZGEiOnt9LCJyYW5kb20iOiIwYTM4MTUwYmQ0MjllY2M4YzliNGM5NTc4NGQ5NjI2MyJ9.aKJePp0mQ6GPKi0Lm5uoaQ-aoMn41x3CVnCF30YKGApFbs9RoA1jhtQr\\_qj7ocOkBIVo-BEN74Qt3uwzOJbbzg](https://zenodo.org/records/16320635?token=eyJhbGciOiJIUzUxMiJ9.eyJpZCI6ImI0OTAzMmM1LTBlZWUtNDU5Mi1hODFiLTc4ZGNmNWJlYmRhNSIsImRhZGEiOnt9LCJyYW5kb20iOiIwYTM4MTUwYmQ0MjllY2M4YzliNGM5NTc4NGQ5NjI2MyJ9.aKJePp0mQ6GPKi0Lm5uoaQ-aoMn41x3CVnCF30YKGApFbs9RoA1jhtQr_qj7ocOkBIVo-BEN74Qt3uwzOJbbzg). Any further information can be requested directly to [manuela.basso@unitn.it](mailto:manuela.basso@unitn.it).

## Acknowledgements

We thank Lorena Pisoni, Martina Greco, Marco Aldrighetti, Valerio Zenatti, Silvia del Longo, and Guendalina Bergonzoni for their technical help. We also thank Prof. Rajiv Ratan, Dr. Marta Biagioli, and Prof. Alberto Inga for insightful comments during the project; Veronica Desanctis and Roberto Bertorelli from the Next-Generation Sequencing Facility at the Department CIBIO, University of Trento, for the library preparations and sequencing; Dr. Jonathan Vinet

(CIGS, University of Modena and Reggio Emilia) and Dr. Ilaria Musante, IRCCS Istituto G. Gaslini, Genova, for technical assistance with imaging analysis; Susan Boerner at the OIST, Okinawa, Japan, for the help with iPSCs culturing. The cryo-EM acquisitions were done at the NoLimits Center of the University of Milan. We want to thank Prof. Magdalena Götz for the Glast-Cre<sup>ERT2</sup> mice. AR acknowledges 'Aldo Ravelli Center for Neurotechnology and Experimental Brain Therapeutics', Università degli Studi di Milano. We thank the ALS patients and control subjects who donated research biosamples. The thumbnail image for the online table of contents was created in BioRender. Basso, M. (2025) <https://BioRender.com/ar0y141>.

## Funding

This project received funding from the European Union's Horizon 2020 research and innovation program under the Marie Skłodowska-Curie grant agreement No 752470 (to M.B.); a grant from the Italian Ministry of Health (GR-2016-02361552 to M.B.); a grant from Ministero dell'Istruzione, dell'Università e della Ricerca (PRIN 20229HKCRT to M.B. and A.R.); a pilot grant from Fondazione AriSLA (SENALS to A.M. and M.B.; EVTestInALS to M.B., A.C., and V.B. and GATTALS to M.B. and V.B.); a grant from Fondazione CARITRO (Bando Postdoc 2020 to A.M.); intramural funding from Department CIBIO, 5X1000 with the project Neurospy; donations from gruppo Rangers GRM Madonnetta and Giovannella Giancarlo; the initiative 'Dipartimenti di Eccellenza 2023–2027 (Legge 232/2016)' funded by the MUR. The Department CIBIO Core Facilities (IRBIO) is supported by the European Regional Development Fund (ERDF) 2014–2020 and 2021–2027. S.I. received a fellowship from the PhD program in 'Experimental Medicine', Università degli Studi di Milano. K.M.B. is supported by a UK Medical Research Council studentship. P.J.S. is supported by the NIHR Sheffield Biomedical Research Centre (NIHR203321). We also acknowledge funding from Italian Ministry of Health project PERMEALS—PNRR-MAD-2022-12375731 (to A.C., V.B., A.R., N.T.), the Department of Excellence grant of the Italian Ministry of University and Research to the 'Rita Levi Montalcini' Department of Neuroscience, University of Torino. G.C. is a PhD student in the Molecular Biomedicine Program of the University of Trieste. S.P. would like to thank the International Center for Genetic Engineering and Biotechnology (ICGEB) for the financial support.

## Competing interests

L.S. is a founder, shareholder and employee of Peptomyc S.L. J.R.W. is a shareholder of Peptomyc S.L.

## Supplementary material

Supplementary material is available at [Brain](https://brain.oup.com/brain/article/149/5/1604/8266576) online.

## References

1. Sofroniew MV. Astrocyte reactivity: Subtypes, states, and functions in CNS innate immunity. *Trends Immunol.* 2020;41: 758–770.
2. Escartin C, Galea E, Lakatos A, et al. Reactive astrocyte nomenclature, definitions, and future directions. *Nat Neurosci.* 2021; 24:312–325.

3. Zimmer TS, Orr AL, Orr AG. Astrocytes in selective vulnerability to neurodegenerative disease. *Trends Neurosci.* 2024;47:289-302.
4. Sofroniew MV. Astroglial pathology. *Cold Spring Harb Perspect Biol.* 2014;7:a020420.
5. Mancardi GL, Liwnicz BH, Mandybur TI. Fibrous astrocytes in Alzheimer's disease and senile dementia of Alzheimer's type: An immunohistochemical and ultrastructural study. *Acta Neuropathol.* 1983;61:76-80.
6. Banati RB, Daniel SE, Blunt SB. Glial pathology but absence of apoptotic nigral neurons in long-standing Parkinson's disease. *Mov Disord.* 1998;13:221-227.
7. Neary D, Snowden JS, Mann DM, Northen B, Goulding PJ, Macdermott N. Frontal lobe dementia and motor neuron disease. *J Neurol Neurosurg Psychiatry.* 1990;53:23-32.
8. Schiffer D, Cordera S, Cavalla P, Migheli A. Reactive astroglial pathology of the spinal cord in amyotrophic lateral sclerosis. *J Neurol Sci.* 1996;139:27-33.
9. Pekny M, Pekna M, Messing A, et al. Astrocytes: A central element in neurological diseases. *Acta Neuropathol.* 2016;131:323-345.
10. Zhang W, Xiao D, Mao Q, Xia H. Role of neuroinflammation in neurodegeneration development. *Sig Transduct Target Ther.* 2023;8:267.
11. Benatar M, Wu J, Huey ED, et al. The Miami framework for ALS and related neurodegenerative disorders: An integrated view of phenotype and biology. *Nat Rev Neurol.* 2024;20:364-376.
12. Hardiman O, Al-Chalabi A, Chio A, et al. Amyotrophic lateral sclerosis. *Nat Rev Dis Primers.* 2017;3:17085.
13. Feldman EL, Goutman SA, Petri S, et al. Amyotrophic lateral sclerosis. *Lancet.* 2022;400:1363-1380.
14. Neumann M, Sampathu DM, Kwong LK, et al. Ubiquitinated TDP-43 in frontotemporal lobar degeneration and amyotrophic lateral sclerosis. *Science.* 2006;314:130-133.
15. Nakashima-Yasuda H, Uryu K, Robinson J, et al. Co-morbidity of TDP-43 proteinopathy in Lewy body related diseases. *Acta Neuropathol.* 2007;114:221-229.
16. Meneses A, Koga S, O'Leary J, Dickson DW, Bu G, Zhao N. TDP-43 Pathology in Alzheimer's disease. *Mol Neurodegener.* 2021;16:84.
17. Garden GA, La Spada AR. Intercellular (mis)communication in neurodegenerative disease. *Neuron.* 2012;73:886-901.
18. Van Harten ACM, Phatnani H, Przedborski S. Non-cell-autonomous pathogenic mechanisms in amyotrophic lateral sclerosis. *Trends Neurosci.* 2021;44:658-668.
19. Rosen DR, Siddique T, Patterson D, et al. Mutations in Cu/Zn superoxide dismutase gene are associated with familial amyotrophic lateral sclerosis. *Nature.* 1993;362:59-62.
20. Yamanaka K, Boillee S, Roberts EA, et al. Mutant SOD1 in cell types other than motor neurons and oligodendrocytes accelerates onset of disease in ALS mice. *Proc Natl Acad Sci U S A.* 2008;105:7594-7599.
21. Boillee S, Yamanaka K, Lobsiger CS, et al. Onset and progression in inherited ALS determined by motor neurons and microglia. *Science.* 2006;312:1389-1392.
22. van Niel G, D'Angelo G, Raposo G. Shedding light on the cell biology of extracellular vesicles. *Nat Rev Mol Cell Biol.* 2018;19:213-228.
23. Gurung S, Perocheau D, Touramanidou L, Baruteau J. The exosome journey: From biogenesis to uptake and intracellular signalling. *Cell Commun Signal.* 2021;19:47.
24. Basso M, Pozzi S, Tortarolo M, et al. Mutant copper-zinc superoxide dismutase (SOD1) induces protein secretion pathway alterations and exosome release in astrocytes. *J Biol Chem.* 2013;288:15699-15711.
25. Marton S, Miquel E, Acosta-Rodríguez J, Fontenla S, Libisch G, Cassina P. SOD1<sup>G93A</sup> astrocyte-derived extracellular vesicles induce motor neuron death by a miRNA-155-5p-mediated mechanism. *ASN Neuro.* 2023;15:17590914231197527.
26. Silverman JM, Christy D, Shyu CC, et al. CNS-derived extracellular vesicles from superoxide dismutase 1 (SOD1)G93A ALS mice originate from astrocytes and neurons and carry misfolded SOD1. *J Biol Chem.* 2019;294:3744-3759.
27. Iguchi Y, Eid L, Parent M, et al. Exosome secretion is a key pathway for clearance of pathological TDP-43. *Brain.* 2016;139:3187-3201.
28. Hung ST, Linares GR, Chang WH, et al. PIKFYVE inhibition mitigates disease in models of diverse forms of ALS. *Cell.* 2023;186:786-802.e28.
29. Ferrara D, Pasetto L, Bonetto V, Basso M. Role of extracellular vesicles in amyotrophic lateral sclerosis. *Front Neurosci.* 2018;12:574.
30. Basso M, Bonetto V. Extracellular vesicles and a novel form of communication in the brain. *Front Neurosci.* 2016;10:127.
31. Arnold ES, Ling SC, Huelga SC, et al. ALS-linked TDP-43 mutations produce aberrant RNA splicing and adult-onset motor neuron disease without aggregation or loss of nuclear TDP-43. *Proc Natl Acad Sci U S A.* 2013;110:E736-E745.
32. Ditsworth D, Maldonado M, McAlonis-Downes M, et al. Mutant TDP-43 within motor neurons drives disease onset but not progression in amyotrophic lateral sclerosis. *Acta Neuropathol.* 2017;133:907-922.
33. Yadav A, Matson KJE, Li L, et al. A cellular taxonomy of the adult human spinal cord. *Neuron.* 2023;111:328-344.e7.
34. Blum JA, Klemm S, Shadrach JL, et al. Single-cell transcriptomic analysis of the adult mouse spinal cord reveals molecular diversity of autonomic and skeletal motor neurons. *Nat Neurosci.* 2021;24:572-583.
35. Lin MC, Lin JJ, Hsu CL, Juan HF, Lou PJ, Huang MC. GATA3 interacts with and stabilizes HIF-1 $\alpha$  to enhance cancer cell invasiveness. *Oncogene.* 2017;36:4243-4252.
36. Brescia P, Schneider C, Holmes AB, et al. MEF2B instructs germinal center development and acts as an oncogene in B cell lymphomagenesis. *Cancer Cell.* 2018;34:453-465.e9.
37. Liu BC, Liu FY, Gao XY, et al. Global transcriptional analyses of the wnt-induced development of neural stem cells from human pluripotent stem cells. *Int J Mol Sci.* 2021;22:7473.
38. Xu K, Qiu C, Pei H, et al. Homeobox B3 promotes tumor cell proliferation and invasion in glioblastoma. *Oncol Lett.* 2018;15:3712-3718.
39. Chen XD, Zhao W, Shen AG. Expression and role of PAK6 after spinal cord injury in adult rat. *Chin J Traumatol.* 2011;14:277-281.
40. Su D, Ellis S, Napier A, Lee K, Manley NR. Hoxa3 and pax1 regulate epithelial cell death and proliferation during thymus and parathyroid organogenesis. *Dev Biol.* 2001;236:316-329.
41. Chen J, Jackson PK, Kirschner MW, Dutta A. Separate domains of p21 involved in the inhibition of Cdk kinase and PCNA. *Nature.* 1995;374:386-388.
42. Qin Y, Sun W, Wang Z, et al. RBM47/SNHG5/FOXO3 axis activates autophagy and inhibits cell proliferation in papillary thyroid carcinoma. *Cell Death Dis.* 2022;13:270.
43. Soleymanjahi S, Blanc V, Molitor EA, et al. RBM47 regulates intestinal injury and tumorigenesis by modifying proliferation, oxidative response, and inflammatory pathways. *JCI Insight.* 2023;8:e161118.
44. Zhang R, Wu Y, Xie F, et al. RGMa mediates reactive astroglial scar formation through TGF $\beta$ 1/Smad2/3 signaling after stroke. *Cell Death Differ.* 2018;25:1503-1516.

45. Schachtrup C, Ryu JK, Helmrick MJ, et al. Fibrinogen triggers astrocyte scar formation by promoting the availability of active TGF- $\beta$  after vascular damage. *J Neurosci*. 2010;30:5843-5854.
46. Endo F, Komine O, Fujimori-Tonou N, et al. Astrocyte-derived TGF- $\beta$ 1 accelerates disease progression in ALS mice by interfering with the neuroprotective functions of microglia and T cells. *Cell Rep*. 2015;11:592-604.
47. Pillai EK, Franze K. Mechanics in the nervous system: From development to disease. *Neuron*. 2024;112:342-361.
48. Pathak MM, Nourse JL, Tran T, et al. Stretch-activated ion channel Piezo1 directs lineage choice in human neural stem cells. *Proc Natl Acad Sci U S A*. 2014;111:16148-16153.
49. Muhamad NA, Masutani K, Furukawa S, et al. Astrocyte-specific inhibition of the primary cilium suppresses C3 expression in reactive astrocyte. *Cell Mol Neurobiol*. 2024;44:48.
50. Mori T, Tanaka K, Buffo A, Wurst W, Kühn R, Götz M. Inducible gene deletion in astroglia and radial glia—A valuable tool for functional and lineage analysis. *Glia*. 2006;54:21-34.
51. Kerkhoff H, Jennekens FGI, Troost D, Veldman H. Nerve growth factor receptor immunostaining in the spinal cord and peripheral nerves in amyotrophic lateral sclerosis. *Acta Neuropathol*. 1991;81:649-656.
52. Nicoletti C, Wei X, Etxaniz U, et al. Muscle denervation promotes functional interactions between glial and mesenchymal cells through NGFR and NGF. *iScience*. 2023;26:107114.
53. Walf AA, Frye CA. The use of the elevated plus maze as an assay of anxiety-related behavior in rodents. *Nat Protoc*. 2007;2:322-328.
54. Bergh S, Casadei N, Gabery S, et al. TDP-43 overexpression in the hypothalamus drives neuropathology, dysregulates metabolism and impairs behavior in mice. *Acta Neuropathol Commun*. 2025;13:119.
55. Reshef YA, Finucane HK, Kelley DR, et al. Detecting genome-wide directional effects of transcription factor binding on polygenic disease risk. *Nat Genet*. 2018;50:1483-1493.
56. van Rheenen W, Shatunov A, Dekker AM, et al. Genome-wide association analyses identify new risk variants and the genetic architecture of amyotrophic lateral sclerosis. *Nat Genet*. 2016;48:1043-1048.
57. Lu T, Aron L, Zullo J, et al. REST and stress resistance in ageing and Alzheimer's disease. *Nature*. 2014;507:448-454.
58. Sleiman SF, Langley BC, Basso M, et al. Mithramycin is a gene-selective Sp1 inhibitor that identifies a biological intersection between cancer and neurodegeneration. *J Neurosci*. 2011;31:6858-6870.
59. Berson A, Sartoris A, Nativio R, et al. TDP-43 Promotes neurodegeneration by impairing chromatin remodeling. *Curr Biol*. 2017;27:3579-3590.e6.
60. Das SK, Lewis BA, Levens D. MYC: A complex problem. *Trends Cell Biol*. 2023;33:235-246.
61. Badia-i-Mompel P, Vélez Santiago J, Braunger J, et al. Decouple R: Ensemble of computational methods to infer biological activities from omics data. *Bioinform Adv*. 2022;2:vbac016.
62. Lagier-Tourenne C, Polymenidou M, Cleveland DW. TDP-43 and FUS/TLS: Emerging roles in RNA processing and neurodegeneration. *Hum Mol Genet*. 2010;19(R1):R46-R64.
63. Chen GS, Chen SY, Liu ST, Hsieh CC, Lee SP, Huang SM. Stabilization of the c-Myc protein via the modulation of threonine 58 and serine 62 phosphorylation by the disulfiram/copper complex in oral cancer cells. *Int J Mol Sci*. 2022;23:9137.
64. Wang X, Cunningham M, Zhang X, et al. Phosphorylation regulates c-Myc's oncogenic activity in the mammary gland. *Cancer Res*. 2011;71:925-936.
65. Yeh E, Cunningham M, Arnold H, et al. A signalling pathway controlling c-Myc degradation that impacts oncogenic transformation of human cells. *Nat Cell Biol*. 2004;6:308-318.
66. Thibodeaux CA, Liu X, Disbrow GL, et al. Immortalization and transformation of human mammary epithelial cells by a tumor-derived Myc mutant. *Breast Cancer Res Treat*. 2009;116:281-294.
67. Meyer K, Ferraiuolo L, Miranda CJ, et al. Direct conversion of patient fibroblasts demonstrates non-cell autonomous toxicity of astrocytes to motor neurons in familial and sporadic ALS. *Proc Natl Acad Sci U S A*. 2014;111:829-832.
68. Ferrer I, Blanco R, Carmona M, Puig B. Phosphorylated c-MYC expression in Alzheimer disease, Pick's disease, progressive supranuclear palsy and corticobasal degeneration. *Neuropathol Appl Neurobiol*. 2001;27:343-351.
69. Guo J, Qiu W, Soh SLY, et al. Motor neuron degeneration in a mouse model of seipinopathy. *Cell Death Dis*. 2013;4:e535-e535.
70. Donini L, Tanel R, Zuccarino R, Basso M. Protein biomarkers for the diagnosis and prognosis of amyotrophic lateral sclerosis. *Neurosci Res*. 2023;197:31-41.
71. Ballabio C, Anderle M, Ganesello M, et al. Modeling medulloblastoma in vivo and with human cerebellar organoids. *Nat Commun*. 2020;11:583.
72. Nilsson JA, Cleveland JL. Myc pathways provoking cell suicide and cancer. *Oncogene*. 2003;22:9007-9021.
73. Soucek L, Helmer-Citterich M, Sacco A, Jucker R, Cesareni G, Nasi S. Design and properties of a myc derivative that efficiently homodimerizes. *Oncogene*. 1998;17:2463-2472.
74. Massó-Vallés D, Soucek L. Blocking Myc to treat cancer: Reflecting on two decades of Omomyc. *Cells*. 2020;9:883.
75. Beaulieu ME, Jauset T, Massó-Vallés D, et al. Intrinsic cell-penetrating activity propels Omomyc from proof of concept to viable anti-MYC therapy. *Sci Transl Med*. 2019;11:eaar5012.
76. Vahsen BF, Nalluru S, Morgan GR, et al. C9orf72-ALS human iPSC microglia are pro-inflammatory and toxic to co-cultured motor neurons via MMP9. *Nat Commun*. 2023;14:5898.
77. La Cognata V, D'Amico AG, Maugeri G, et al. CXCR2 is deregulated in ALS spinal cord and its activation triggers apoptosis in motor neuron-like cells overexpressing hSOD1-G93A. *Cells*. 2023;12:1813.
78. Perner C, Perner F, Stubendorff B, et al. Dysregulation of chemokine receptor expression and function in leukocytes from ALS patients. *J Neuroinflammation*. 2018;15:99.
79. Annunziata I, van de Vlekkert D, Wolf E, et al. MYC competes with Mit/TFE in regulating lysosomal biogenesis and autophagy through an epigenetic rheostat. *Nat Commun*. 2019;10:3623.
80. Shao W, Todd TW, Wu Y, et al. Two FTD-ALS genes converge on the endosomal pathway to induce TDP-43 pathology and degeneration. *Science*. 2022;378:94-99.
81. Beckers J, Van Damme P. Toxic gain-of-function mechanisms in C9orf72 ALS-FTD neurons drive autophagy and lysosome dysfunction. *Autophagy*. 2024;20:2102-2104.
82. Kilinc S, Paisner R, Camarda R, et al. Oncogene-regulated release of extracellular vesicles. *Dev Cell*. 2021;56:1989-2006.e6.
83. Adams SD, Csere J, D'angelo G, et al. Centrosome amplification mediates small extracellular vesicle secretion via lysosome disruption. *Curr Biol*. 2021;31:1403-1416.e7.
84. Latifkar A, Ling L, Hingorani A, et al. Loss of sirtuin 1 alters the secretome of breast cancer cells by impairing lysosomal integrity. *Dev Cell*. 2019;49:393-408.e7.
85. van de Vlekkert D, Demmers J, Nguyen XX, et al. Excessive exosome release is the pathogenic pathway linking a lysosomal deficiency to generalized fibrosis. *Sci Adv*. 2019;5:eaav3270.

86. Barbo M, Ravnik-Glavač M. Extracellular vesicles as potential biomarkers in amyotrophic lateral sclerosis. *Genes (Basel)*. 2023;14:325.
87. Mathieu M, Martin-Jaular L, Lavieu G, Théry C. Specificities of secretion and uptake of exosomes and other extracellular vesicles for cell-to-cell communication. *Nat Cell Biol*. 2019;21:9-17.
88. van Niel G, Carter DRF, Clayton A, Lambert DW, Raposo G, Vader P. Challenges and directions in studying cell-cell communication by extracellular vesicles. *Nat Rev Mol Cell Biol*. 2022;23:369-382.
89. Welsh JA, Goberdhan DCI, O'Driscoll L, et al. Minimal information for studies of extracellular vesicles (MISEV2023): From basic to advanced approaches. *J Extracell Vesicles*. 2024;13:e12404.
90. Weber B, Sturm R, Henrich D, Marzi I, Leppik L. CD44+ and CD31+ extracellular vesicles (EVs) are significantly reduced in polytraumatized patients with hemorrhagic shock—Evaluation of their diagnostic and prognostic potential. *Front Immunol*. 2023;14:1196241.
91. Buffo A, Rite I, Tripathi P, et al. Origin and progeny of reactive gliosis: A source of multipotent cells in the injured brain. *Proc Natl Acad Sci U S A*. 2008;105:3581-3586.
92. Buffo A, Rolando C, Ceruti S. Astrocytes in the damaged brain: Molecular and cellular insights into their reactive response and healing potential. *Biochem Pharmacol*. 2010;79:77-89.
93. Zelic M, Blazier A, Pontarelli F, et al. Single-cell transcriptomic and functional studies identify glial state changes and a role for inflammatory RIPK1 signaling in ALS pathogenesis. *Immunity*. 2025;58:961-979.e8.
94. D'Erchia AM, Gallo A, Manzari C, et al. Massive transcriptome sequencing of human spinal cord tissues provides new insights into motor neuron degeneration in ALS. *Sci Rep*. 2017;7:10046.
95. Humphrey J, Venkatesh S, Hasan R, et al. Integrative transcriptomic analysis of the amyotrophic lateral sclerosis spinal cord implicates glial activation and suggests new risk genes. *Nat Neurosci*. 2023;26:150-162.
96. Tam OH, Rozhkov NV, Shaw R, et al. Postmortem cortex samples identify distinct molecular subtypes of ALS: Retrotransposon activation, oxidative stress, and activated Glia. *Cell Rep*. 2019;29:1164-1177.e5.
97. Ziff OJ, Clarke BE, Taha DM, Crerar H, Luscombe NM, Patani R. Meta-analysis of human and mouse ALS astrocytes reveals multi-omic signatures of inflammatory reactive states. *Genome Res*. 2022;32:71-84.
98. Ceyzériat K, Abjean L, Carrillo-de Sauvage MA, Ben Haim L, Escartin C. The complex STATes of astrocyte reactivity: How are they controlled by the JAK-STAT3 pathway? *Neuroscience*. 2016;330:205-218.
99. Patani R, Hardingham GE, Liddelow SA. Functional roles of reactive astrocytes in neuroinflammation and neurodegeneration. *Nat Rev Neurol*. 2023;19:395-409.
100. Richardson PJ, Smith DP, De Giorgio A, et al. Janus kinase inhibitors are potential therapeutics for amyotrophic lateral sclerosis. *Transl Neurodegener*. 2023;12:47.
101. Milani M, Della Valle I, Rossi S, et al. Neuroprotective effects of niclosamide on disease progression via inflammatory pathways modulation in SOD1-G93A and FUS-associated amyotrophic lateral sclerosis models. *Neurotherapeutics*. 2024;21:e00346.
102. Sutherland KD, Vaillant F, Alexander WS, et al. c-myc as a mediator of accelerated apoptosis and involution in mammary glands lacking Socs3. *EMBO J*. 2006;25:5805-5815.
103. Farrell AS, Sears RC. MYC degradation. *Cold Spring Harb Perspect Med*. 2014;4:a014365.
104. Cargnello M, Roux PP. Activation and function of the MAPKs and their substrates, the MAPK-activated protein kinases. *Microbiol Mol Biol Rev*. 2011;75:50-83.
105. Chung YH, Joo KM, Lim HC, et al. Immunohistochemical study on the distribution of phosphorylated extracellular signal-regulated kinase (ERK) in the central nervous system of SOD1G93A transgenic mice. *Brain Res*. 2005;1050:203-209.
106. Bendotti C, Atzori C, Piva R, et al. Activated p38MAPK is a novel component of the intracellular inclusions found in human amyotrophic lateral sclerosis and mutant SOD1 transgenic mice. *J Neuropathol Exp Neurol*. 2004;63:113-119.
107. Gibbs KL, Kalmar B, Rhymes ER, et al. Inhibiting p38 MAPK alpha rescues axonal retrograde transport defects in a mouse model of ALS. *Cell Death Dis*. 2018;9:596.
108. Zhou Y, Liu X, Ma S, et al. Chk1 activation induces reactive astrogliosis through CIP2A/PP2A/STAT3 pathway in Alzheimer's disease. *FASEB J*. 2022;36:e22209.
109. Mertens J, Herdy JR, Traxler L, et al. Age-dependent instability of mature neuronal fate in induced neurons from Alzheimer's patients. *Cell Stem Cell*. 2021;28:1533-1548.e6.
110. Wong GCN, Chow KHM. DNA damage response-associated cell cycle re-entry and neuronal senescence in brain aging and Alzheimer's disease. *J Alzheimers Dis*. 2023;94(s1):S429-S451.
111. Di Giovanni S, Movsesyan V, Ahmed F, et al. Cell cycle inhibition provides neuroprotection and reduces glial proliferation and scar formation after traumatic brain injury. *Proc Natl Acad Sci U S A*. 2005;102:8333-8338.
112. Porterfield V, Khan SS, Foff EP, et al. A three-dimensional dementia model reveals spontaneous cell cycle re-entry and a senescence-associated secretory phenotype. *Neurobiol Aging*. 2020;90:125-134.
113. Nguyen MD, Boudreau M, Kriz J, Couillard-Després S, Kaplan DR, Julien JP. Cell cycle regulators in the neuronal death pathway of amyotrophic lateral sclerosis caused by mutant superoxide dismutase 1. *J Neurosci*. 2003;23:2131-2140.
114. Barbosa LF, Cerqueira FM, Macedo AFA, et al. Increased SOD1 association with chromatin, DNA damage, p53 activation, and apoptosis in a cellular model of SOD1-linked ALS. *Biochim Biophys Acta*. 2010;1802:462-471.
115. Farg MA, Konopka A, Soo KY, Ito D, Atkin JD. The DNA damage response (DDR) is induced by the C9orf72 repeat expansion in amyotrophic lateral sclerosis. *Hum Mol Genet*. 2017;26:2882-2896.
116. Lopez-Gonzalez R, Lu Y, Gendron TF, et al. Poly(GR) in C9ORF72-related ALS/FTD compromises mitochondrial function and increases oxidative stress and DNA damage in iPSC-derived motor neurons. *Neuron*. 2016;92:383-391.
117. Qiu H, Lee S, Shang Y, et al. ALS-associated mutation FUS-R521C causes DNA damage and RNA splicing defects. *J Clin Invest*. 2014;124:981-999.
118. Giannini M, Bayona-Feliu A, Sproviero D, Barroso SI, Cereda C, Aguilera A. TDP-43 mutations link amyotrophic lateral sclerosis with R-loop homeostasis and R loop-mediated DNA damage. *PLoS Genet*. 2020;16:e1009260.
119. Maor-Nof M, Shipony Z, Lopez-Gonzalez R, et al. P53 is a central regulator driving neurodegeneration caused by C9orf72 poly(PR). *Cell*. 2021;184:689-708.e20.
120. Haidet-Phillips AM, Gross SK, Williams T, et al. Altered astrocytic expression of TDP-43 does not influence motor neuron survival. *Exp Neurol*. 2013;250:250-259.
121. Serio A, Bilican B, Barmada SJ, et al. Astrocyte pathology and the absence of non-cell autonomy in an induced pluripotent stem cell model of TDP-43 proteinopathy. *Proc Natl Acad Sci U S A*. 2013;110:4697-4702.

122. Moujalied D, Grubman A, Acevedo K, et al. TDP-43 mutations causing amyotrophic lateral sclerosis are associated with altered expression of RNA-binding protein hnRNP K and affect the Nrf2 antioxidant pathway. *Hum Mol Genet.* 2017;26:1732-1746.
123. Rojas F, Cortes N, Abarzua S, Dyrda A, van Zundert B. Astrocytes expressing mutant SOD1 and TDP43 trigger motoneuron death that is mediated via sodium channels and nitroxidative stress. *Front Cell Neurosci.* 2014;8:24.
124. Ponta H, Sherman L, Herrlich PA. CD44: From adhesion molecules to signalling regulators. *Nat Rev Mol Cell Biol.* 2003;4:33-45.
125. Beers DR, Zhao W, Wang J, et al. ALS patients' regulatory T lymphocytes are dysfunctional, and correlate with disease progression rate and severity. *JCI Insight.* 2017;2:e89530.
126. Golia MT, Frigerio R, Pucci S, et al. Changes in glial cell activation and extracellular vesicles production precede the onset of disease symptoms in transgenic hSOD1G93A pigs. *Exp Neurol.* 2024;374:114716.
127. Kang SH, Li Y, Fukaya M, et al. Degeneration and impaired regeneration of gray matter oligodendrocytes in amyotrophic lateral sclerosis. *Nat Neurosci.* 2013;16:571-579.
128. Philips T, Bento-Abreu A, Nonneman A, et al. Oligodendrocyte dysfunction in the pathogenesis of amyotrophic lateral sclerosis. *Brain.* 2013;136:471-482.
129. Edgar R. Gene expression omnibus: NCBI gene expression and hybridization array data repository. *Nucleic Acids Res.* 2002;30:207-210.
130. Perez-Riverol Y, Bandla C, Kundu DJ, et al. The PRIDE database at 20 years: 2025 update. *Nucleic Acids Res.* 2025;53(D1):D543-D553.